

Abschlussarbeit zur Erlangung des akademischen Grades  
Master of Science

# **Waves in lipid layers**

David Hannes

22. Dezember 2017

Medizinische und Biologische Physik  
Lehrstuhl für Experimentelle Physik IV  
Fakultät für Physik  
Technische Universität Dortmund

Erstgutachter dieser Arbeit ist Prof. Dr. Matthias F. Schneider.  
Zweitgutachter ist Prof. Dr. Metin Tolan.

---

## Abstract

Acoustic waves are discussed as the physical foundation of action potentials. Such waves have been confirmed in lipid mono- and bilayers. However it is unclear, if these observations can be transferred to biological tissues. Therefore, this thesis uses stacked lipid layers to investigate emerging waves in a tissue model.

Thermodynamic forces - namely temperature and electric fields - were used to excite stacked lipid layers. For temperature an emerging wave at the phase transition temperature was observed in bright-field and fluorescence microscopy. A non-diffusive propagation characteristic was found for this wave ( $x \propto t^\alpha$ , with  $0.8 \leq \alpha \leq 1.8$ ). The response of the stacked lipids to electrical fields changed distinctively upon passage of this wave. Its speed is in the range of 2 mm/min – 15 mm/min.

The morphological similarities of the model with biological tissues suggest that observed phenomena in the lipid layers are expected to be found in real tissues, too. Indeed, the speed of spreading depression (SD) waves is similar (2 mm/min – 9 mm/min). SD waves are associated with migraine and a breakdown of transmembrane ion gradients [1]. As well as a depression of spontaneous activity [2] in grey matter.

This substantial change of membrane properties during a SD wave is similar to the change of membrane properties during the waves presented here. Those changes imply that the lipid layers undergo a phase transition.

A physical foundation of waves which propagate in a tissue-like model has been presented. This makes it likely that similar waves propagate in biological tissue. The potential relation to spreading depression was discussed and could be critically tested by recording the lipid phase state in grey matter during a SD wave.

## Kurzfassung

Akustische Wellen stehen in der Diskussion Aktionspotentiale durch einen rein physikalischen Ansatz erklären zu können. Sie wurden bereits in Lipidmonolagen und Lipiddoppelschichten gefunden. Allerdings ist nicht geklärt, ob sich diese Ergebnisse auch auf biologische Gewebe übertragen lassen. Deswegen wurden in dieser Arbeit Wellen in Lipidstapeln untersucht.

Die Lipidstapel wurden mit thermodynamischen Kräften - elektrischen Feldern und Temperaturgradienten - angeregt, mit dem Ziel eine Welle anzulösen. Im Falle eines Temperaturgradienten konnte eine propagierende Welle nahe des Phasenübergangs im Durch- und Fluoreszenzlichtmikroskop beobachtet werden. Die elektrische Erregbarkeit der Stapel änderte sich deutlich mit dem propagieren der Welle. Außerdem zeigte sich ihr nicht diffusives Verhalten ( $x \propto t^\alpha$ , mit  $0.8 \leq \alpha \leq 1.8$ ). Die Geschwindigkeiten lagen im Bereich von 2 mm/min – 15 mm/min.

Lipidstapel zeigen eine große morphologische Ähnlichkeit zu biologischen Gewebe. Entsprechend ist es naheliegend, dass Phänomene, die in diesem Modell entdeckt

---

werden, mit großer Wahrscheinlichkeit auch in biologischen Gewebe zu finden sind. Tatsächlich, werden ähnliche Geschwindigkeiten (2 mm/min – 9 mm/min) bei sogenannten Streudepolarisationswellen (SD Wellen) beobachtet.

SD Wellen werden in Zusammenhang mit Migräne gebracht und ein Zusammenbruch des Transmembranionengradientens [1] ist beobachtbar. Zusätzlich wird eine Depression der spontanen elektrischen Aktivität [2] in der grauen Substanz gemessen. Diese tiefgreifende Änderungen der Membraneigenschaften während der Welle sind vergleichbar mit den Änderungen in den Lipidstapeln während der Propagation der hier beobachteten Welle. Die Eigenschaftsänderungen legen nahe, dass es sich um eine propagierende Phasenumwandlung handelt.

Die präsentierten Phasenumwandlungswellen sind vollständig durch einen physikalischen Ansatz erklärbar. Es ist wahrscheinlich, dass vergleichbare Wellen auch in biologischem Gewebe zu finden sind. Der Zusammenhang, der zu Streudepolarisationswellen gefunden wurde, könnte in zukünftigen Experimenten kritisch überprüft werden. Dafür sollte der Phasenzustand der Lipide in der grauen Substanz während einer SD Welle gemessen werden.

## List of Figures

2.1	Chemical structure of the phospholipids DMPC and DPPC. . . . .	5
2.2	Cross section of different aggregates of phospholipids in an aqueous medium. . . . .	6
2.3	Specific heat capacity versus temperature for lipid vesicles of different mole fractions of the lipids DMPC and DPPC. . . . .	8
2.4	Light microscopy of muscle tissue and schematic drawings for explanation. . . . .	11
2.5	Section of the human brain showing grey and white matter. . . . .	12
2.6	Layers in grey matter in different stains. . . . .	13
2.7	Schematic drawings of the different kinds of epithelial tissue. . . . .	14
2.8	Schematic drawing of bone tissue. . . . .	15
2.9	The excitation and emission spectra of Texas Red. . . . .	16
3.1	PTFE separator of the experimental chamber. . . . .	20
3.2	ITO slides and PTFE separator clipped into the copper block. . . . .	20
3.3	Spin coater SCC 200 from Novocontrol Technologies. . . . .	22
3.4	Pictures with emerging wave and their differences. . . . .	25
3.5	Median of the wave and movement analysis. . . . .	26
4.1	DMPC lipid layers under bright-field microscopy. . . . .	28
4.2	Bright-field microscopy before and after electroformation. . . . .	28
4.3	Fluorescence microscopy of lipid layers with Texas Red after electroformation. . . . .	29
4.4	Fluorescence microscopy of spin-coated lipid layers with Texas Red. . . . .	31
4.5	Emerging wave in spin-coated lipids. . . . .	32
4.6	Mean intensities of pictures while wave propagates. . . . .	33
4.7	Generalized polarization of Laurdan in DMPC layers prepared by solvent evaporation. . . . .	36
4.8	Generalized polarization live recording in DMPC layers made by solvent evaporation. . . . .	36
4.9	Texas Red spectra measurement and intensities for different temperatures. . . . .	37
4.10	Non-processed median propagation. . . . .	40
4.11	Slope calculation for DMPC while heating. . . . .	41
4.12	Slope calculation for DMPC while cooling. . . . .	41



## List of Tables

4.1	Selection of temperature values when the wave emerges. . . . .	35
4.2	Intensities at 609 nm for different temperatures in spin-coated DMPC sample. . . . .	38
4.3	Examples of wave velocities for DMPC and DPPC. . . . .	39



# Contents

<b>1</b>	<b>Introduction</b>	<b>1</b>
<b>2</b>	<b>Theory</b>	<b>3</b>
2.1	Thermodynamics . . . . .	3
2.2	Lipids . . . . .	5
2.2.1	Structure of phospholipids . . . . .	5
2.2.2	Phase transition in lipids . . . . .	6
2.2.3	Diffusion and waves . . . . .	9
2.3	Tissues . . . . .	11
2.3.1	Muscle tissue . . . . .	11
2.3.2	Nervous tissue . . . . .	12
2.3.3	Epithelial tissue . . . . .	14
2.3.4	Connective tissue . . . . .	15
2.4	Fluorescence microscopy . . . . .	16
2.4.1	Fluorescence and its application . . . . .	16
2.4.2	Generalized polarization . . . . .	17
<b>3</b>	<b>Material and methods</b>	<b>19</b>
3.1	Lipids and dyes . . . . .	19
3.2	Experimental set-up . . . . .	19
3.3	Preparation of multilayers . . . . .	21
3.3.1	Solvent evaporation . . . . .	21
3.3.2	Spin-coating . . . . .	21
3.4	Electroformation . . . . .	22
3.5	Spectrum analysis . . . . .	23
3.6	Automatic wave front tracking . . . . .	24
<b>4</b>	<b>Results</b>	<b>27</b>
4.1	Formation and characterization of multilayers . . . . .	27
4.1.1	Solvent evaporation . . . . .	27
4.1.2	Spin-coating . . . . .	30
4.2	Effects of thermodynamic forces . . . . .	31
4.2.1	Electric fields . . . . .	31
4.2.2	Temperature . . . . .	32
4.3	Wave propagation at phase transition . . . . .	34
4.3.1	Thermal threshold of lipid chain length . . . . .	34
4.3.2	Indication by dyes . . . . .	35

## Contents

---

4.4	Propagation velocity and behaviour . . . . .	38
4.4.1	Velocity . . . . .	38
4.4.2	Non-diffusive behaviour . . . . .	39
<b>5</b>	<b>Discussion</b>	<b>43</b>
5.1	Layer counts . . . . .	43
5.2	Necessary prerequisites . . . . .	43
5.3	Thermodynamic forces . . . . .	45
5.4	Varying wave speeds for DMPC and DPPC . . . . .	46
5.5	Comparable phenomena . . . . .	47
5.5.1	Spreading depression waves . . . . .	47
5.5.2	Supercooling of water . . . . .	48
<b>6</b>	<b>Conclusion</b>	<b>51</b>

# 1 Introduction

Describing and understanding nature were the goals of physicists ever since. Many ground breaking results in physics have helped improving our understanding of the world around us and made our daily lives more comfortable and save. Using physics to explain biological systems is comparatively new. The first time the term biophysics was introduced was in 1892 [3]. From this point on many achievements have been accomplished in biophysics by researchers from many different backgrounds.

One famous example is the attempt to describe communication in nerve cells with electric pulses by Hodgkin and Huxley in 1952 [4]. They measured changes in the electrical potential of membranes and interpreted these observations in a fully electric model. In this context the term action potential is used, allowing to describe the typical all-or-none behaviour, the velocity and the propagation of the electrical potential changes. For these changes ion-specific molecules are assumed that allow ions to pass the membrane. For their groundbreaking work Hodgkin and Huxley were awarded the Nobel Prize in Physiology or Medicine in 1963.

Recent research has shown that a fully electric model is - at least - insufficient as not only changes in the electric potential of the membrane can be measured but also reversible heat changes [5], changes in optical [6] and mechanical [7] properties have been recorded during an action potential.

At this point the idea of describing this phenomenon in a different way came up. Thermodynamics offers a description that is able to reproduce not only the electrical results, but also includes the changes in many different properties. Using thermodynamics seems to be reasonable because “it is the only physical theory of universal content which I am convinced will never be overthrown.”, as Einstein states in his autobiographical notes [8]. The laws of thermodynamics are able to describe a very broad range of phenomena. Especially for biological systems a thermodynamic approach seems promising as these systems strongly depend on a wide range of different variables such as temperature, pH, pressure and other stresses.

Applying this approach to 2D lipid bilayers Konrad Kaufmann argued that action potentials are propagating pulses, similar to sound in 2D [9–11]. These pulses are excited near a transition and hence able to show the typical ‘all-or-none’ behaviour. Since the description of action potentials as acoustic density pulses, this group already performed many experiments on mono- and bilayers and could reproduce the predictions of this theory [12–14].

## 1 Introduction

---

One main reason for working with monolayers is that they represent a controllable interface. Interfaces are dominating in cells and biological tissues. At this point the question occurs if these findings are also observable in tissues or organs. The idea is to stack lipid bilayers to mimic the behaviour of tissues.

It will become clear that a property all tissues have in common is their constitution. Most tissues are built up by stacks of cells, justifying to use this model in a first approach. Here the stacks of lipid layers are excited by thermodynamic forces. The reactions are recorded with a microscope. This method reveals information about the ongoing processes and underlying physical principles. One major point will be an emerging wave accompanied by a transition (similar to an ordered-unordered phase transition) during heating and cooling the lipid multilayers. This wave has so far not been observed in a tissue-like model. It shows characteristics similar to the so called spreading depression [2]. Spreading depression is a phenomenon in the human cortex that is associated with migraine.

Comparing the waves found here with this example, it will be shown the immanent possibility to explain phenomena in living systems with basic laws of physics. Additionally, in another example supercooled water will be investigated. The idea is to apply the same physical approach that explains biological functions in spreading depression, in order to show the universality of propagating perturbations. It will be pointed out that the similar mechanisms are appropriate to describe the phenomenon, although not every question can be fully answered in this thesis.

## 2 Theory

Here the argumentation for the found waves in lipid layers will be motivated. Therefore a few theoretical considerations have to be taken into account. First the underlying principles of thermodynamics and its implications will be presented before the focus will be put on the biological aspects. An introduction to lipids and their characteristics in layers will be given. Furthermore lipid layers as a simple model for tissues will be exemplified.

### 2.1 Thermodynamics

Looking at biological systems from a thermodynamic point of view is a promising approach for understanding and describing organisms, and life in general. The idea is that physical laws are universal and hence apply to biology in particular. Many findings do not take thermodynamics as a physical basis into account to explain the respective phenomena. An example is the phenomenon of action potentials in nerve pulses, which are described in an all electrical model. This thesis will start from the second law of thermodynamics in the interpretation of Clausius:

$$\oint dS = 0. \quad (2.1)$$

This means that entropy  $S$  can formally be interpreted as a conservative physical potential. Consequently, entropy only depends on extensive variables as for example volume  $V$ , energy  $E$  or charge  $Q$ . For simplification entropy will only depend on one external variable  $S(x)$  in the following, but can easily be extended to multiple variables. Expanding entropy around its maximum at  $x = \bar{x} = 0$  as a Taylor series gives

$$S \approx S_0 + \frac{\partial S}{\partial x}x + \frac{1}{2} \frac{\partial^2 S}{\partial x^2}x^2. \quad (2.2)$$

Since entropy is expanded at its maximum, its first derivatives disappear ( $\partial S/\partial x = 0$ ) and the second derivatives are negative ( $\partial^2 S/\partial x^2 < 0$ ). This mathematical claim has a physical explanation. Entropy is maximal at equilibrium meaning no resulting forces act on the thermodynamic system, this can be found in the disappearing first derivatives as they represent thermodynamic forces. The second derivatives do not disappear, meaning that even at equilibrium fluctuations can be observed and

## 2 Theory

---

thermodynamic properties are changing (slightly). Now entropy can be expressed as

$$S = S_0 - \frac{1}{2}\beta x^2, \quad (2.3)$$

with  $\beta = \frac{\partial^2 S}{\partial x^2}$  as a positive constant. In the next step this equation will be combined with Boltzmann's statistical description of entropy:

$$S = k_B \ln w, \quad (2.4)$$

where  $k_B$  is the Boltzmann constant and  $w$  is the probability of the system being in a defined state. The major challenge of this Boltzmann's description is to find a complete molecular model to calculate the probability  $w$ . Without this molecular model the equation does not fulfill a purpose as Einstein pointed out 1910 [15]. But the equation can be inversed (Einstein's inversion [15]) to:

$$w = \text{const.} \times e^{S(x)}, \quad (2.5)$$

enabling to measure the thermodynamic susceptibilities of a system. Those susceptibilities are linked to entropy, making it possible to calculate the probabilities for single states. Substitution of eq. 2.3 in eq. 2.5 gives a probability distribution [16]:

$$w(x) dx = A e^{-\frac{1}{2}\beta x^2} dx, \quad (2.6)$$

with the normalization constant  $A$ , which can be determined to  $A = \sqrt{\beta/2\pi}$  by integration over all probabilities  $\int w(x) dx = 1$ .

This distribution has the form of a Gaussian distribution, so eq. 2.6 can be rewritten as

$$w(x) dx = \frac{1}{\sqrt{2\pi \langle x^2 \rangle}} e^{-\frac{x^2}{2\langle x^2 \rangle}} dx, \quad (2.7)$$

with the mean square fluctuation  $\langle x^2 \rangle = \int_{-\infty}^{\infty} x^2 w(x) dx = \beta^{-1}$ . At this point the consequences of these considerations are shortly discussed. Starting from the second law of thermodynamics it was shown that entropy can be expanded as a potential leading to a Gaussian distribution of a thermodynamic variable  $x$ . This Gaussian distribution already implies fluctuations which are inherently present and that can be determined mathematically. Consequently, in every thermodynamic system fluctuations appear and might be measured. The magnitude of fluctuations can be seen in the shape of the distribution. Small fluctuations  $\langle x^2 \rangle$  are found with a sharp maximum of  $w$  and vice versa. Most importantly the variable  $x$  can be any extensive variable of interest, e.g. charge  $Q$ , volume  $V$  or even the internal energy  $U$ . This leads to a *full* description and understanding of complex biological systems. The right set of thermodynamic variables allows to model the influences on the biological system by pH, electric fields, magnetic fields, temperature and so on. This full description cannot be provided by any other known theory in means of fundamental validity and applicability.

## 2.2 Lipids

Coming from the fundamental laws of thermodynamics now the more experimental components are described. The first component are lipids, which are the building blocks of membranes. In the context of this thesis phospholipids are of special interest because they are the most prevalent lipids in the membrane [17].

### 2.2.1 Structure of phospholipids

Phospholipids are esterified lipids with a phosphoric acid group [18]. Figure 2.1 shows the chemical structure of the two phospholipids used in this thesis. On top there is dimyristoylphosphatidylcholine (DMPC) shown and on the bottom dipalmitoylphosphatidylcholine (DPPC) is displayed.

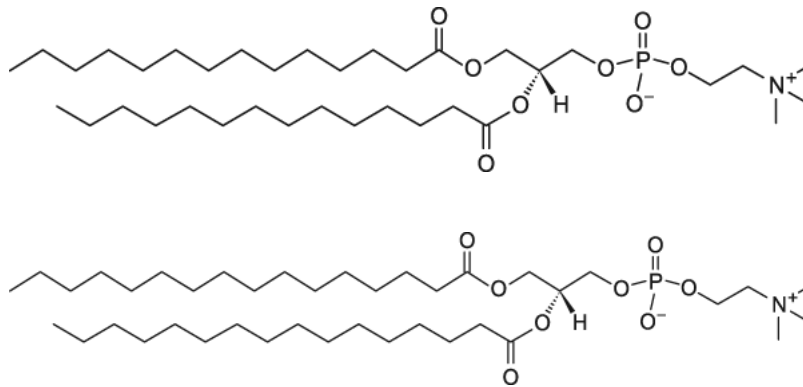


**Figure 2.1:** Chemical structure of the phospholipids DMPC (top) and DPPC (bottom) [19].

DMPC and DPPC show a similar structure. They both have a phosphoric acid group with a negatively charged oxygen ion and a positively charged choline group. Those two local charges make those phospholipids zwitterionic, which means that they do not show an overall charge but are locally charged. The only difference of DMPC and DPPC is the length of their fatty acid chains. Where a DMPC chain consists of 14 carbon atoms, 16 carbon atoms are found in a DPPC chain. This difference is displayed in the melting temperatures  $T_m$  of the lipids. DMPC has a melting temperature of  $T_m^{\text{DMPC}} = 24^\circ\text{C}$ , whereas the melting temperature of DPPC is  $T_m^{\text{DPPC}} = 41^\circ\text{C}$  [19]. Phospholipids show the special characteristic of being amphiphil, which means that one part of molecule is hydrophobic and the other part is hydrophilic. In these cases the phosphate group is the hydrophilic 'head' and the fatty acid chains are the hydrophobic 'tails' [17]. When in aqueous media the lipids build special aggregates as liposomes, micelles or bilayers (see figure 2.2).

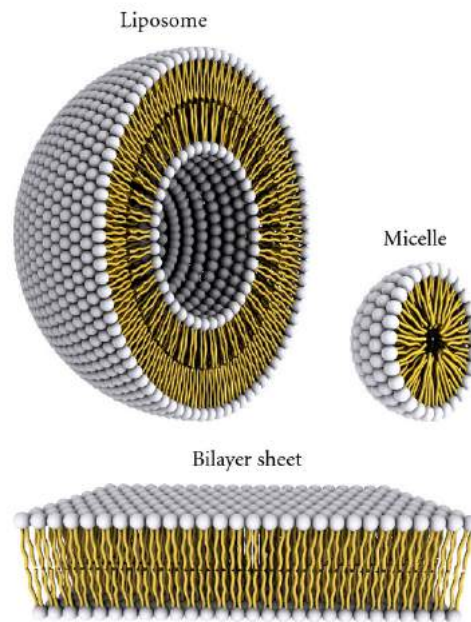


**Figure 2.2:** Cross section of different aggregates of phospholipids in an aqueous medium. The white spheres represent the hydrophilic head groups and the yellow tubes represent the hydrophobic tails of the phospholipid [20].

The formation of aggregates with a distinct structure is called self-organization and states a major difference to e.g. proteins. There no self-organization is found. Those aggregates can be found in the human body. Bilayers are employed as cell membranes, liposomes are used for intercellular transport of molecules as so called vesicles. Micelles form for digestion and absorption of fat. In the human body these aggregates often have a more complex structure with linked proteins or sugars. But in principle they are built up by lipids.

### 2.2.2 Phase transition in lipids

Lipids in aggregates as presented in figure 2.2 behave as thermodynamic systems. In general thermodynamic systems can undergo phase transitions, especially for those lipid aggregates presented this is well known [21, 22]. Here the connection of the thermodynamic approach to biological systems (section 2.1) and phase transitions in lipids is made. The thermodynamic system of lipids can be described by the entropy potential. If it shows phase transitions, this implies a special shape of the potential where multiple maxima are present. Each maximum represents a different phase. By letting thermodynamic forces (= first derivatives of entropy) act on the system, the position in the potential can be changed leading to phase transitions. Most notable is the behaviour of thermodynamic susceptibilities at phase transition.

Thermodynamic susceptibilities are measurable quantities representing the fluctuations of entropy. They are expressed through the second derivatives of entropy and connected to the fluctuations by

$$\langle x^2 \rangle = -k_B \left( \frac{\partial^2 S}{\partial x^2} \right)^{-1}, \quad (2.8)$$

analogous to the mean square fluctuations in equation 2.7<sup>1</sup>, with  $k_B$  the Boltzmann constant. The thermodynamic susceptibility heat capacity at constant pressure  $C_p$  will be given as an example to show the behaviour of fluctuations at phase transitions. The associated energy to  $C_p$  is the enthalpy  $H$  which can be expressed as:

$$H = C_p T$$

where  $T$  is the temperature. With the little trick of setting  $\gamma = 1/T$  it can be followed that

$$\left. \frac{\partial H}{\partial \gamma} \right|_p = -\frac{1}{\gamma^2} C_p,$$

solved for  $C_p$ :

$$C_p = -\gamma^2 \left. \frac{\partial H}{\partial \gamma} \right|_p = -\gamma^2 \left( \left. \frac{\partial \gamma}{\partial H} \right|_p \right)^{-1} = -\gamma^2 \left( \left. \frac{\partial}{\partial H} \frac{\partial S}{\partial H} \right|_p \right)^{-1} = -\gamma^2 \left( \left. \frac{\partial^2 S}{\partial H^2} \right|_p \right)^{-1}$$

Combining this result with equation 2.8 leads to

$$C_p = \frac{\langle H^2 \rangle}{k_B T^2} \quad (2.9)$$

The heat capacity for constant pressure is a measurable variable to directly determine the fluctuations of enthalpy. Looking at the results from calorimetry measurements [23] the characteristics of fluctuations can directly be observed. Figure 2.3 shows the temperature dependency of the heat capacity of vesicles made from different mixtures of DMPC:DPPC. For the respective transition temperatures of the pure lipid vesicles (see subsection 2.2.1) maxima of  $c_p = C_p/N$ , with the Avogadro number  $N$  are noticeable. These maxima show that at phase transition the fluctuations behave highly non-linear. Also, the absolute values of the (specific) heat capacity have their maximum at phase transition, as well.

<sup>1</sup>the factor  $k_b$  is included in the constant of equation 2.5, and therefore not explicitly presented in equation 2.7.

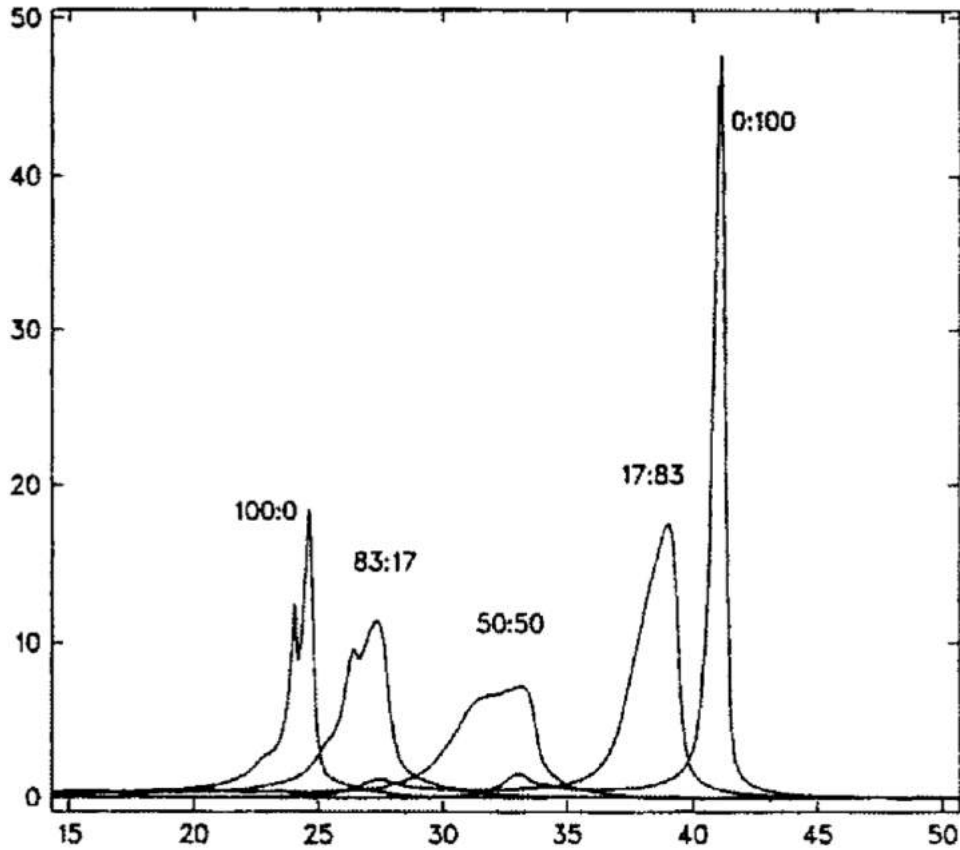


**Figure 2.3:** Specific heat capacity  $c_p$  (kJ/molK) versus temperature  $T$  ( $^{\circ}\text{C}$ ) for lipid vesicles of different mole fractions of the lipids DMPC:DPPC, modified from [23].

To illustrate the universal validity analogous calculations lead to the electric capacity  $C_{el}$  as the thermodynamic susceptibility for the fluctuations of the charge  $q$  [24]:

$$C_{el} = \frac{\langle q^2 \rangle}{k_B T} \quad (2.10)$$

This shows that thermodynamic susceptibilities are not limited to mechanical quantities but can cover all physical observables. The most important feature of the fluctuations is their non-linear behaviour as it opens many possibilities to new phenomena at phase transition.

One major finding in the context are acoustic pulses in lipid monolayers [25–27]. They are able to explain complex biological processes with thermodynamics. This work will show that another interesting process can be found in lipid layers which has not been described so far.

At this point it should be clearly stated that for the findings the term phase transition is used for convenience. At no point it will be discussed what kind of special

transition is observed (first order, second order etc.) and there is no necessity to give these processes a specific name. The main point is a non-linear change in observables that are directly connected to fluctuations.

### 2.2.3 Diffusion and waves

In this part the description of transportation processes in lipid layers in particular and biological systems in general will be discussed. In biology transportation phenomena a distinction is made between two cases, transport can either be active or passive. An active transport includes an adequate infrastructure and a constant energy supply. An example might be motor proteins in the cell that need adenosine triphosphate (ATP) to move along microtubules. Those proteins are thereby able to move cargo actively in the cell. Passive transport is generally described by diffusion. Diffusion is the movement of particles caused by the likelihood of their current position [?]. Analogous to the idea in section 2.1 the position of particles in an ensemble fluctuates. If particles are externally pushed into a unlikely state (e.g. by adding a drop of ink to water), they will start moving in order to reach a more likely state. This behaviour can be mathematically described by Fick's Law

$$\vec{j} = -D \text{grad } \rho_N, \quad (2.11)$$

with  $\vec{j}$  the particle flux,  $D$  the diffusion constant and  $\rho_N$  the particle density. With the help of the continuity equation

$$\frac{\partial \rho_N}{\partial t} + \text{div } \vec{j} = 0, \quad (2.12)$$

where  $t$  is time, the diffusion equation can be derived

$$\frac{\partial \rho_N}{\partial t} - D \Delta \rho_N = 0, \quad (2.13)$$

with the Laplace operator  $\Delta$ . Solutions in three dimensions of equation 2.13 are of the form:

$$\rho(x, y, z, t) = \sqrt{\left(\frac{1}{4\pi Dt}\right)^3} e^{-\frac{x^2+y^2+z^2}{4Dt}}. \quad (2.14)$$

This equation has the form of a Gaussian distribution. The width of the curve is determined by  $4Dt$ , which implies an increase of the width by time. At the same time the value at the centre decreases with  $t^{-3/2}$ . Looking at the time development of a point following this dynamic process the typical behaviour can be seen [28]:

$$x \propto \sqrt{Dt} \quad (2.15)$$

## 2 Theory

---

The relation makes it possible to decide whether a process is diffusive or not. Therefore it is necessary to plot the distance  $x$  on a double logarithmic scale as a function of time  $t$ . Calculating the slope of the resulting line gives information about the diffusive behaviour:

$$\log(x) = \log(\sqrt{2Dt}) = \frac{1}{2} \log(t) + b, \quad (2.16)$$

with  $b = \log(\sqrt{2D}) = \text{const.}$ <sup>2</sup> and the slope  $m = \frac{1}{2}$ . If the measurable slope is of a different value than  $\frac{1}{2}$ , the process is not diffusive.

Taking the results of this group on acoustic waves in lipid monolayers [25–27], the concept of using waves for explaining communication in cells seems to be appropriate to be further explored. Since the phenomena found here are waves in lipid multilayers, a brief introduction to waves will be given.

A wave is a periodically propagation of a disturbance in space and time. In the case of linear propagating disturbances in one dimension the wave equation is given by

$$\frac{\partial^2 u}{\partial t^2} = c^2 \frac{\partial^2 u}{\partial x^2}, \quad (2.17)$$

with the speed of sound  $c$ , time  $t$ , dimension  $x$  and the disturbance  $u$ . The mathematical form of this equation differs from the the diffusion equation. The speed of sound does not depend on time but is characterized by  $c = \sqrt{\frac{\partial p}{\partial \rho}}$ , with pressure  $p$  and density  $\rho$ . Comparing these waves with diffusion in the double logarithmic plot, it can be seen that the slope is different. Diffusive processes show a slope of  $m = 0.5$ , whereas linear waves lead to a slope of  $m = 1$ . This makes it possible to decide whether the wave is of diffusive or ballistic nature:

$$\log(x) = \log(ct) = \log(t) + b, \quad (2.18)$$

with  $b = \log(c) = \text{const.}$  and the slope  $m = 1$ . As an example for a linear wave, an acoustic wave in air will be given. With the premise of small pressure perturbations  $p$ , equation 2.17 can be transformed to:

$$\frac{\partial^2 p}{\partial t^2} = c^2 \frac{\partial^2 p}{\partial x^2}. \quad (2.19)$$

In the case of constant temperature the velocity is calculated to:

$$c = \sqrt{\left(\frac{\partial p}{\partial \rho}\right)\bigg|_T} = \sqrt{\frac{RT_0}{M}} \approx 290 \text{ m/s}, \quad (2.20)$$

with  $R = 8.314\,472 \text{ J}/(\text{mol K})$  the ideal gas constant,  $T_0 = 293.15 \text{ K}$  the ambient temperature and  $M = 0.028\,965 \text{ kg/mol}$  the molecular weight of air.

<sup>2</sup>The proportionality constant in equation 2.15 is taken from Einstein [?].

## 2.3 Tissues

In the introduction it was stated that the focus of this work is to investigate the behaviour of lipid layers under thermodynamic forces. These lipid layers are employed as a simple model for tissue. It will be shown that tissues are generally built up by stacks of cells, which is why this model is employed. This is done analogously to the model of mono- and bilayers mimicking single cells.

In general a tissue is an ensemble of similar cells that is held together by an extracellular matrix and intercellular contacts [29]. In the following different tissues will be described to emphasize the structural constitution of tissues as stacks of cells. A general distinction is being drawn between four groups of tissue: muscle tissue, nervous tissue, epithelial tissue and connective tissue.

### 2.3.1 Muscle tissue

Muscles are needed every day for simple movements as well as for complex motions. Muscle tissue can be divided into three groups **a** skeletal muscle, **b** cardiac muscle, and **c** smooth muscle (figure 2.4).

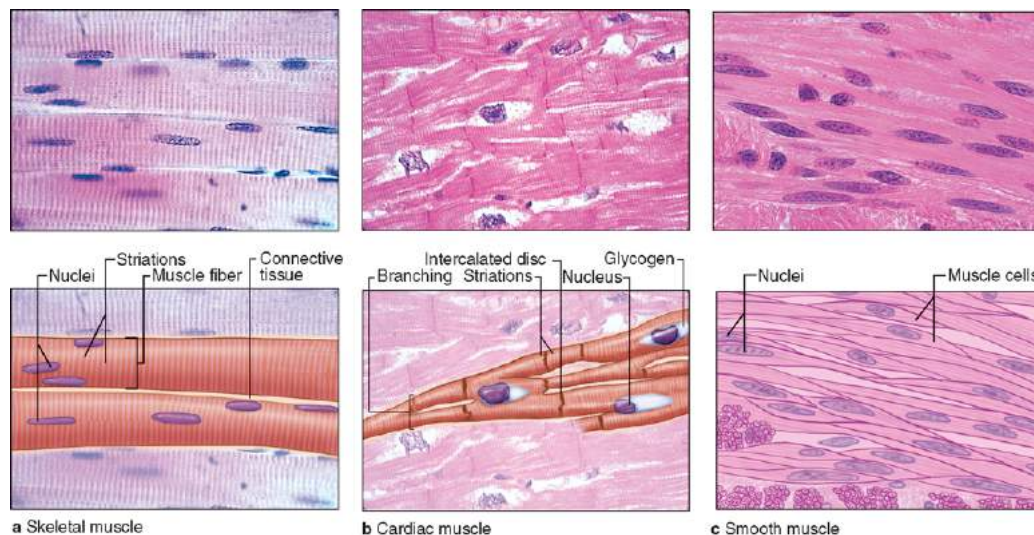


**Figure 2.4:** Light microscopy of muscle tissue and schematic drawings for explanation. **a** shows a skeletal muscle with large fibres that have multiple nuclei and the typical striation (magnification 200x). **b** shows a cardiac muscle with its irregular branch structure being connected by intercalated discs and glycogen that is stored in the muscle (magnification 200x). **c** shows a smooth muscle with its fusiform characteristics where every cell has a single nucleus and no striations (magnification 300x). The dense intercellular packing can be recognized by the small amount of extracellular connective tissue. Modified from [30].

## 2 Theory

---

In light microscopy it can be directly seen that muscle cells are closely connected to each other, showing a stacked-like constitution. Considering the fact that muscles show this structure in all 3 dimensions, for example to build the human heart, it can be easily followed that muscle tissue is a great example of stacks of cells and fibres. This result confirms the assumption of using lipid layers as a model for muscle tissue.

### 2.3.2 Nervous tissue

The brain plays a major role in the understanding how the human body works and how different parts of the body communicate with each other. The concept of communication via neurons sending electrical signals is well understood and widely accepted. Nonetheless not all communication is moderated electrically as for example hormones play an important role in cell communication, too. The brain can be histologically divided into two parts, the grey and white matter [31]. In most cases grey matter is the superficial part as it can be seen in figure 2.5.

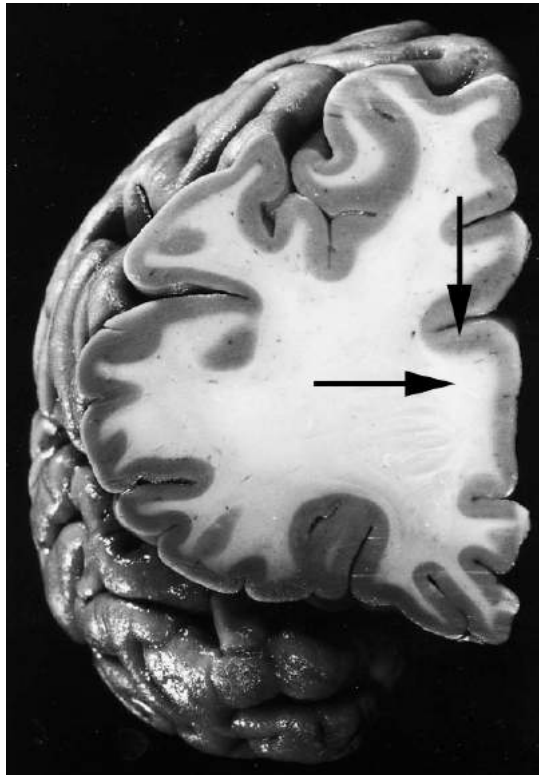


**Figure 2.5:** Section of the human brain. Arrows indicate grey and white matter (substantia grisea and substantia alba). Arrow pointing to the right indicates white and arrow pointing to the bottom indicates grey matter, modified from [32].

Grey matter itself can be categorized into different layers as presented in figure 2.6. This categorization already supports the idea of using lipid multilayers to mimic the behaviour of tissues. It can be seen that a low orientation of cells already satisfy the requirements for a tissue. From this it can be derived that a high orientation of lipid layers is not strongly necessary. Those lipid layers might also be embedded in a not oriented surrounding.

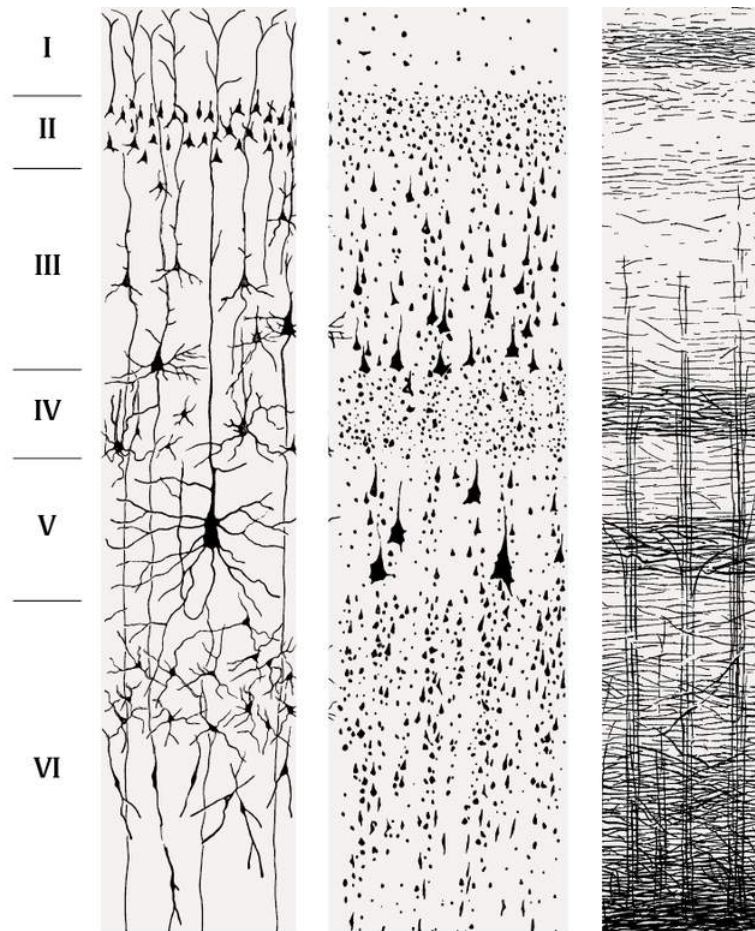


**Figure 2.6:** Layers in grey matter shown in different stains. From left to right: Golgi stain, Nissl stain and myelin stain. The different layers are I molecular layer, II external granule cell layer, III external pyramidal cell layer, IV internal granule cell layer, V internal pyramidal cell layer, VI multiform layer, modified from [31].

### 2.3.3 Epithelial tissue

Epithelial tissue is the most impressive example to show the layer-like constitution of a tissue. A schematic drawing of the different types of epithelial tissue is shown in figure 2.7.

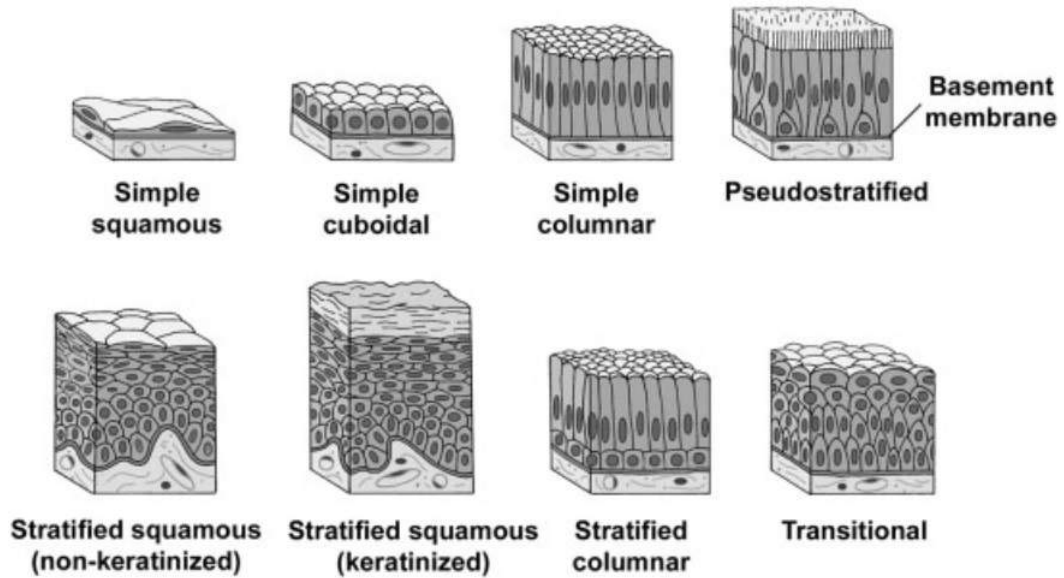


**Figure 2.7:** Schematic drawings of the different kinds of epithelial tissue. A general distinction is made between cells of single layer (simple) and multiple layers (stratified). Also the epithelium might have an extra layer of keratin (keratinized) to protect it from abrasion or other stresses [33].

The epithelial cells are always attached to a base membrane and are connected to each other by different types of junctions. Differences can be found in the number of layers. The simple form consists of one layer of cells, whereas the stratified form has multiple layers. The pseudo forms of each general constitution can be found in the body, too. An example is the pseudostratified form, that is present in the respiratory tract. Cells of different heights are found there but only the tallest cells reach the free surface.

Additionally, a layer of keratin gives extra protection against abrasion and other stress factors in keratinized epithelium. The special case of stratified epithelium cells clearly shows the idea of using multiple lipid layers to mimic tissue constitution. But also the simple forms are covered by the model because they are attached to a basement membrane, which is built up by layers of lipids, as well.

### 2.3.4 Connective tissue

Connective tissue is a difficult case to show a general constitution, as its components and specific forms vary widely in the body. In all cases three main components can be found: fibres, cells and the ground substance. The ground substance is a gel-like substance in the extracellular space. Here the example of bone tissue will be given to illustrate the constitution of connective tissue.

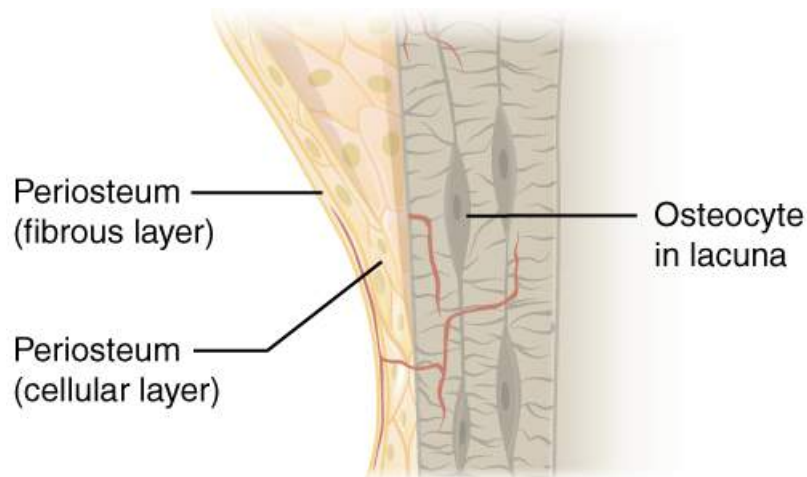


**Figure 2.8:** Schematic drawing of bone tissue. The outer structure of a long bone is shown. Additionally the periosteum which covers the bone matrix is displayed. The bone matrix is built up by osteoblasts, that secret collagen to build the bones. In this process the osteoblasts get captured in the matrix in little oblong spaces (lacunae). When they cannot move, they switch to their inactive form and are called osteocytes, modified from [34].

In figure 2.8 the periosteum is shown in a schematic drawing. The periosteum consists of layers of fibres on top of layers of cells, that cover the actual bone matrix. These extra layers of cells show the stack-like constitution of a tissue.

It should be mentioned that the bone matrix itself does not consist of layers of lipids. Nonetheless, the periosteum is found in all bones which makes it an important feature of bone tissue and cannot be left out. Therefore the model of using lipid layers to mimic tissues can be confirmed.

## 2.4 Fluorescence microscopy

In this section the basics of fluorescence are explained and the specific characteristics of fluorescence microscopy are illustrated by the example of Texas Red.

### 2.4.1 Fluorescence and its application

Fluorescence is a special case of luminescence. Luminescence describes the process of an electronically excited system, that relaxes under the emission of light [35]. This emission can either start directly (reaction time  $\tau_R < 10^{-8}$  s) with maximal intensity or might take some time ( $\tau_R > 10^{-8}$  s) and the intensity increases over time to its maximum value. In the first case the luminescence immediately stops as soon as the excitation stops. In the latter case the material is still emitting photons after the excitation has stopped. Fluorescence is described with the first case. Phosphorescence is the latter case.

In life sciences fluorescence is more convenient. The instant and specific emission of photons makes it possible to track the activity of for example enzymes. A fluorescent dye is characterized by its excitation and emission spectra. The fluorescent dyes used here are Laurdan and Texas Red. An example of the spectrum of Texas Red is shown in figure 2.9.

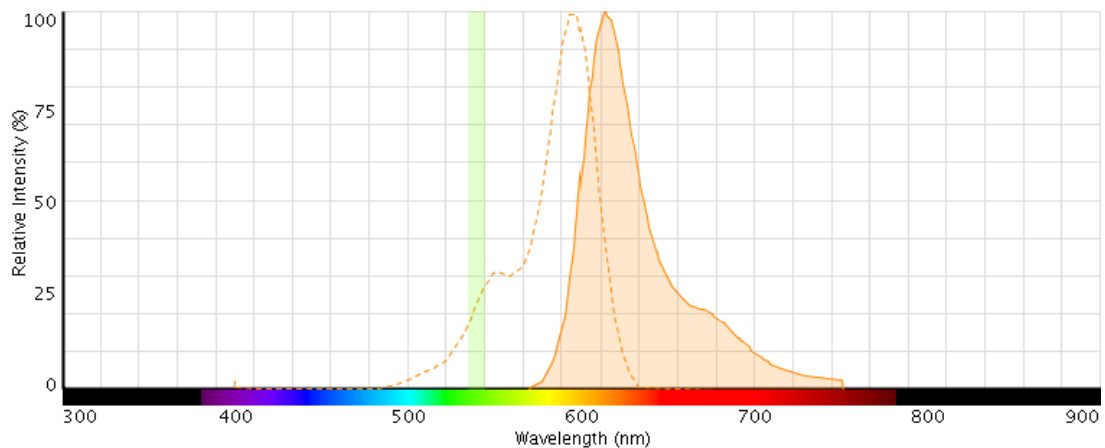


**Figure 2.9:** The excitation (dashed curve) and emission (orange curve) spectra of Texas Red. Additionally the used excitation filter (530 nm – 550 nm) is shown in green [36]. Additionally a 590 nm long pass is employed as an emission filter, that is not displayed.

Most significant is the fact that the dye is excited by a different wavelength than it emits. This phenomenon is called Stokes shift, named after its discoverer George Gabriel Stokes in 1852 [37]. Its cause is the loss of energy to different vibrational states in the molecules [35].

Nonetheless, the excitation and emission wavelengths overlap partly, which is why filters are employed to distinguish the signals. In the set-up used here the sample is excited by light of wavelengths between 530 nm – 550 nm causing the dye to emit photons. In order to register only the photons that were emitted a 590 nm long pass emission filter is employed.

The resulting image is either observed directly with a microscope or recorded with a spectrometer. It was shown that dyes couple to the lipid layers, changing according to changes in the stack [12]. This is required since the changing properties of the dyes are investigated to observe the behaviour of the lipid layers in different situations.

## 2.4.2 Generalized polarization

The fluorescence polarization of biological samples is a key feature that is investigated in many studies [38–40]. It deploys information on the different states of the lipids in a bilayer [41]. To measure the polarization equation 2.21 is employed [35]

$$P = \frac{I_{\parallel} - I_{\perp}}{I_{\parallel} + I_{\perp}}, \quad (2.21)$$

where  $I_{\parallel}$  and  $I_{\perp}$  are the intensity of the parallel respectively horizontally polarized emission and  $P$  is the polarization. A huge drawback of measuring the polarization is that for every point in the image a whole spectrum has to be recorded to obtain information about the phase of the lipids in the bilayer. A way to avoid this is to introduce the generalized polarization

$$GP = \frac{I_B - I_R}{I_B + I_R}, \quad (2.22)$$

where  $I_B$  and  $I_R$  are the fluorescence intensities measured for two different wavelengths. The indices indicate the wavelength of the respective intensity. The index (B) denotes a wavelength in the blue part of the spectrum and the index (R) denotes a wavelength in the red part of the spectrum. General polarization represents the emission spectrum in a single parameter [35].

Its definition is analogous to the fluorescence polarization in (2.21), so it fulfills important properties of the classical polarization [41]. Other advantages of general polarization are that it does not need calibration [42] and it is independent on fluorescence dye concentration in the sample [43]. By calculating the generalized polarization of a dye phase transitions are indicated in lipids, which will be investigated later (see subsection 4.3.2).



## 3 Material and methods

### 3.1 Lipids and dyes

The lipids, used in the experiments, are dipalmitoylphosphatidylcholine (DPPC) with a transition temperature of 41 °C and dimyristoylphosphatidylcholine (DMPC) with a transition temperature of 24 °C [19]. All lipids (purity > 99 %) were purchased from Avanti, USA in a chloroform solution with a concentration of 25 mg/mL. This stock solution is further diluted with chloroform (purity  $\geq$  99.8 % for HPLC amylene stabilized) from Sigma-Aldrich, Germany to a final concentration of 10 mg/mL. The employed dyes are 6-Dodecanoyl-N,N-dimethyl-2-naphthylamine (Laurdan) from Sigma-Aldrich, Germany with a purity of  $\geq$  97 % (HPLC), Texas Red DHPE from Thermofisher, USA diluted in chloroform.

For the production of some lipid multilayers (see section 3.3) 2,2,2-Trifluoroethanol (TFE) with a purity of  $\geq$  99.8 % from Carl Roth GmbH & Co. KG was employed.

### 3.2 Experimental set-up

The experimental set-up consists of a chamber that is clipped to a copper block. Two square (25 mm  $\times$  25 mm) indium tin oxide coated glass slides (ITO slides) are used as a substrate. The ITO slides are taken to allow electrical stimulation of the lipid layers. Hence, the conducting sites of the ITO slides have to face each other. In order to build a chamber, a separator or spacer for the ITO slides is needed. Figure 3.1 shows the employed separator. It is made from Polytetrafluorethylen (PTFE) and has a height of 2 mm. Additionally, two inlets of 0.4 mm (denoted as shaded 'tubes' in figure 3.1) are drilled into the spacer. The idea is to use these inlets to fill the chamber with a buffer solution to mimic the conditions in the human body. Another characteristic of the spacer are the two 4 mm  $\times$  4 mm gaps which are used to attach alligator clamps to the ITO slides. This is necessary for the production of vesicles on the surface which will be further explained in section 3.4.

In order to stabilize this set-up the chamber is clipped into a copper block that can be heated and cooled with an thermoelectric element (Peltier element). This Peltier element is attached to the large copper area (see figure 3.2). For heating or cooling currents of different polarity are employed.

### 3 Material and methods

---

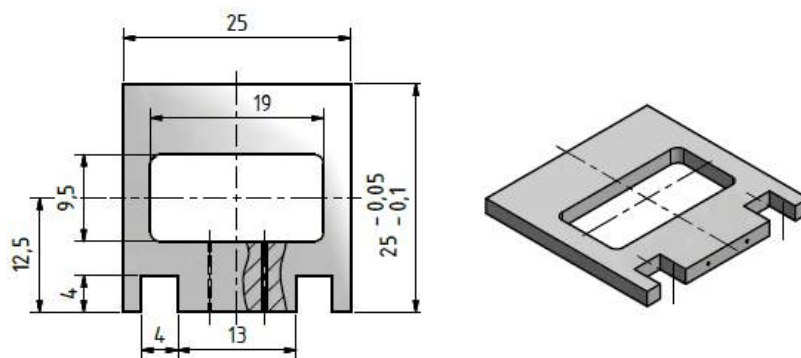


**Figure 3.1:** PTFE separator of the experimental chamber. All dimensions displayed in mm.

The heating respective cooling rate varies significantly with different ambient temperatures. Also in most cases an extra cooling/heating of the Peltier element was done. Therefore it is impossible to give a specific value. All temperature recordings are done with a MAX6675 thermocouple attached to an arduino or a TENMA 72-7715 thermometer. The thermo sensitive sites are placed on top of the upper ITO slide for measuring the temperature. All observations are recorded with a Hamamatsu DCAM camera employed in a Olympus IX71 inverted fluorescence microscope. The software HoKaWo 2.10 is used to save pictures and videos of the samples. For recording every 200 ms or 500 ms a pictures is taken.

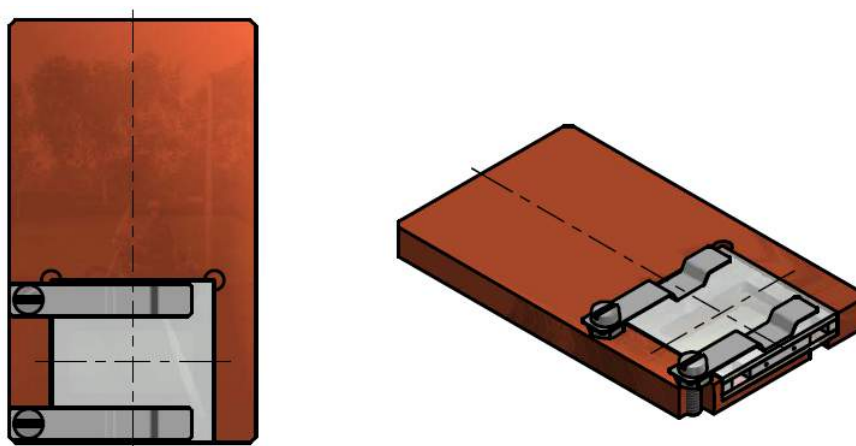


**Figure 3.2:** ITO slides and PTFE separator clipped into the copper block. No dimensions shown for better overview.

## 3.3 Preparation of multilayers

Different methods are used to produce multilayers of varying layer numbers. For many multilayers (a few hundred) the solvent evaporation procedure of Seul and Sammon [44] that was enhanced by Khattari [45] is used. For approximately 9-17 multilayers Spin-Coating described by Mennecke and Salditt [46] is employed. In both cases ITO slides with a resistivity of  $70 \Omega/\text{sq}$ - $100 \Omega/\text{sq}$  from sigma-aldrich are used as a substrate.

To clean the substrate it is sonicated for 30 minutes in isopropanol and after that sonicated for another 30 minutes in bidistilled water before it is dried under a stream of  $\text{N}_2$ . Cleaned substrates are stored in Petri dishes in the refrigerator at  $4^\circ\text{C}$ .

### 3.3.1 Solvent evaporation

For the solvent evaporation the lipid concentration of the sample is set to  $10 \text{ mg/ml}$  in a solution of (1:1 vol/vol) chloroform and TFE. Further more  $1\%$  of the respective dye is added. Different volumes ( $200 \mu\text{l}$ - $500 \mu\text{l}$ ) of the final solution have to be pipetted on the conducting side of an ITO slide. At the point of pipetting the glass slide has to be as plane as possible so the lipid solution can distribute equally all over the slide to form homogeneous lipid stacks. Right after applying the solution the ITO slides have to be covered (e.g. with a cake dome) to avoid fast evaporation of the solvent. After 1.5h the ITO slides have to be put in a vacuum over night evaporate the remaining solvent. To observe the lipid stacks an ITO slide with the dried lipid layers and a clean ITO slide are built to the chamber as described in section 3.2. When clipped into the copper block the lipid layers are rehydrated with bi-distilled water applied by a syringe through the inlets until the chamber is flooded with water.

In some cases after the rehydration the lipid layers went under electroformation (see section 3.4) to produce giant unilamellar vesicles (GUV) which are attached to the lipid stack surface. This makes it easier to observe the ongoing phenomena under the microscope.

### 3.3.2 Spin-coating

For the Spin-Coating the lipid concentration of the sample is set to  $10 \text{ mg/ml}$  and the respective dye is added with a concentration of  $\lesssim 1\%$ . Additionally to the usual cleaning, the ITO slides are stored in  $2 \text{ g/l}$  NaOH solution overnight. The NaOH solution enhances the hydrophilic characteristics of the ITO slide surface. For spin-coating the spin coater SCC 200 from Novocontrol Technologies was employed (see figure 3.3).

The ITO slide is placed on top of the small metal stage and the vacuum pump is

### 3 Material and methods

---

turned on. A little outlet in the metal stage, that is connected to the vacuum pump produces a local vacuum, stabilizing the ITO slide. For a uniform distribution of the lipids during spinning it is essential to place the substrate centric on the stage. The lipids are slowly added with a syringe in small drops with a total volume of approximately 700  $\mu\text{l}$ .

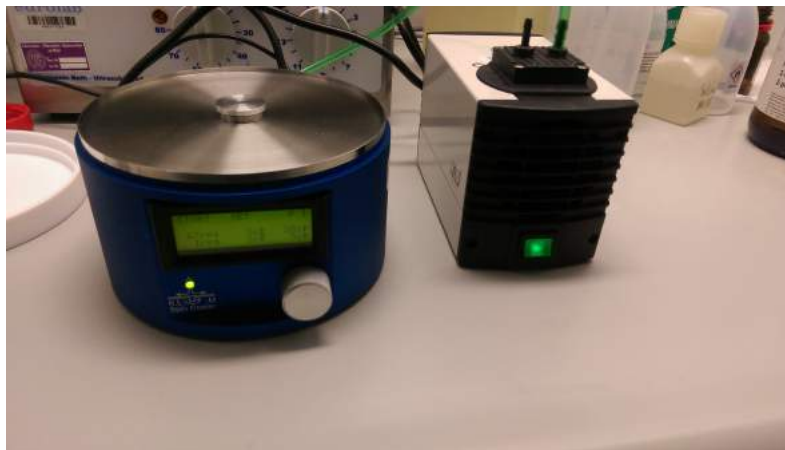


**Figure 3.3:** Front view of spin coater SCC 200 from Novocontrol Technologies. On the right side the vacuum pump for stabilizing the substrate is shown. On the left a part of a covering white cap is visible.

The aim is to fully cover the surface of the substrate with the lipid solution. The rotation of the stage follows a simple protocol. The substrate with lipid covered surface is accelerated to a final speed of 67 rps in 3 s. The substrate will be rotated at the speed of 67 rps for 30 s and after that slowed down to 1 rps in 3 s and rotated at this speed for another 3 s before stopping. The stage and cover are cleaned with chloroform before the first and after each coating.

## 3.4 Electroformation

Electroformation is a method for producing giant unilamellar vesicles (GUV). It was first introduced by Angelova [47]. This technique is employed with a frequency of 10 Hz and 1.5 V for at least 1.5 h.

For electroformation two electrodes are attached to either of the ITO slides of the chamber. On the conducting side of the bottom slide the lipids are already added as described in section 3.3 and the chamber is filled with bidistilled water. Now 1.5 V with 10 Hz are applied for at least 1.5 h.

## 3.5 Spectrum analysis

During the experiments different dyes are applied to display the ongoing processes in the lipid layers. Those dyes also reveal information about the thermodynamic state of the lipids as it will become clear in subsection 4.3.2. To take advantage of this characteristic the spectra of lipid layers containing the respective dye will be recorded.

Therefore the spectrometer 'C10083CA Mini-spectrometer TM series' from Hamamatsu is used. The set-up is placed in a water filled beaker which temperature is controlled by a water bath. The surrounding water of the set-up allows to control temperature accurately ( $\pm 0.2^\circ\text{C}$ ) and offers a homogeneous temperature distribution avoiding temperature gradients. The temperature of the water bath is set by an internal control and externally checked with an external thermometer that is put into the beaker.

After setting the respective temperature the set-up is given 10 min to equilibrate. When the temperature is equilibrated 10 or 100 spectra with an integration time of 100 ms for each spectrum are taken. Those 10 or 100 spectra are averaged, the standard deviations are calculated and used for errorbars in the plots. The resulting spectra are either plotted directly or the intensity values of a specific wavelength is shown for different temperatures. The third possibility is calculating the generalized polarization from equation 2.22 and display it as a function of temperature.

Generalized polarization was only employed for Laurdan, since changes in the lipids are displayed by a shift in the spectrum. The investigated wavelengths for generalized polarization are  $I_B = 450\text{ nm}$  and  $I_R = 500\text{ nm}$ . Those three methods reveal more information about the thermodynamic state of the lipids layers.

In some cases live-measurements are taken. A live-measurement is performed on the normal set-up from section 3.2. During such a measurement only one spectrum every 100 ms is taken with an integration time of 100 ms, while the chamber is heated or cooled. Simultaneously, the temperature is recorded as described in section 3.2. The temperature measurement is started at the same time as the first spectrum measurement. This allows to assign each spectrum a specific temperature.

## 3.6 Automatic wave front tracking

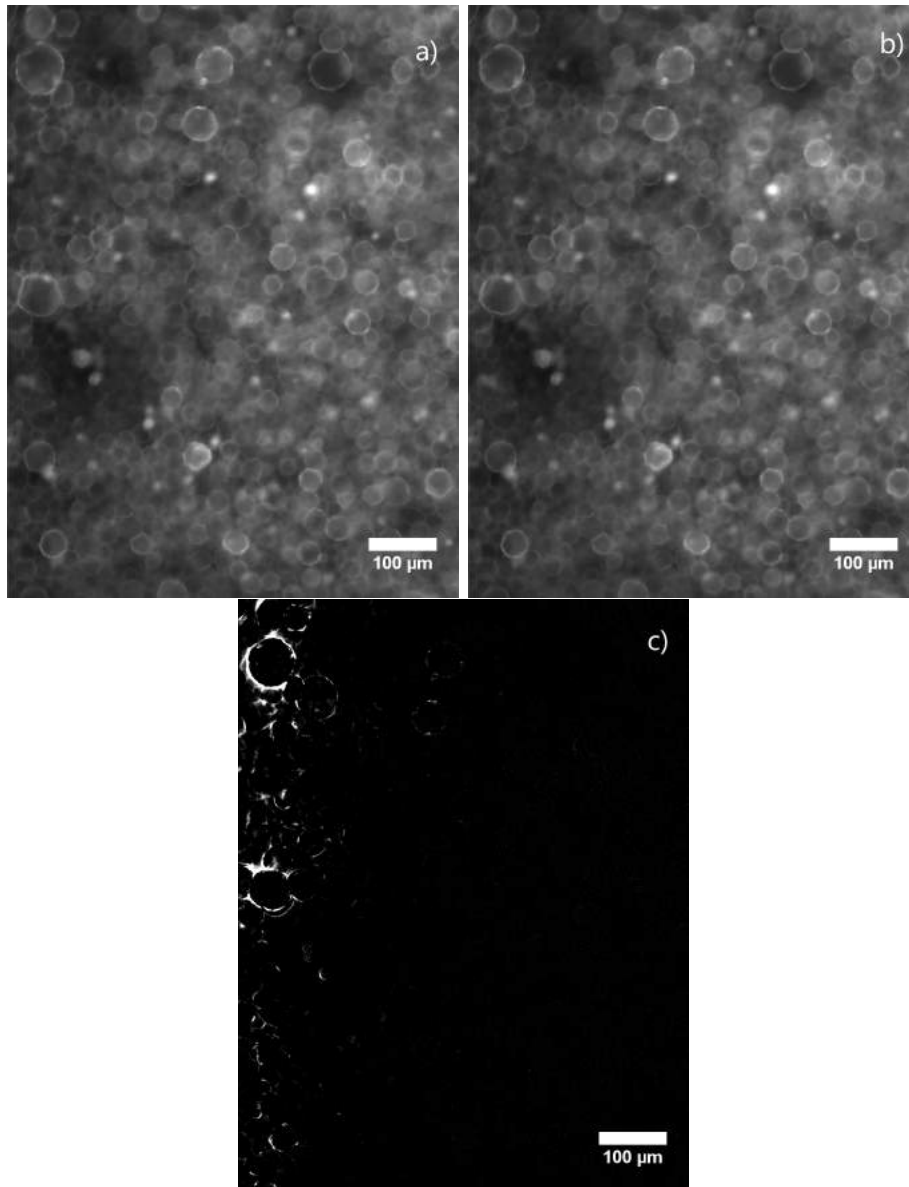
In the next chapter (Results) a propagation of a wave will be observed. In order to decide about the wave propagation behaviour as explained in subsection 2.2.3 the wave has to be tracked and plotted versus time. During the wave the picture is changing locally. This fact will be used to investigate the propagation. The idea is to subtract each picture from the precursor and only show those parts of the resulting picture that differ significantly from each other. This process is illustrated in an example.

Figure 3.4 shows two pictures where a wave emerges which is difficult to see in the single picture. Therefore the difference of the pictures is presented. To calculate the differences each pixel in both pictures is taken and compared. If the difference of those pixels is above a certain threshold, the specific pixel is plotted white otherwise it is plotted black. The positions of the white pixels are saved and the median is calculated to the respective axis. A video of the movement of the differences can be found here<sup>1</sup>. The median is chosen because the average is very sensitive to outliers. In this case the wave emerges from left to right, so the median is calculated in means of the horizontal (x axis) values. Figure 3.5 shows the picture a) from figure 3.4 with the differences plotted as blue points and the calculated median in orange.

Additionally, the time development of the median is shown in a double logarithmic plot. To verify the wave front behaviour, the slope for the measured median values is calculated. For comparison the slopes  $m_1 = 0.5$  and  $m_2 = 1$  are shown.

---

<sup>1</sup>[https://youtu.be/Uv\\_5BZXQFzk](https://youtu.be/Uv_5BZXQFzk)



**Figure 3.4:** Two consecutive (a, b) pictures with the emerging wave. In each picture the wave is not recognizable but when calculating the difference (c) the effect of the wave becomes visible.

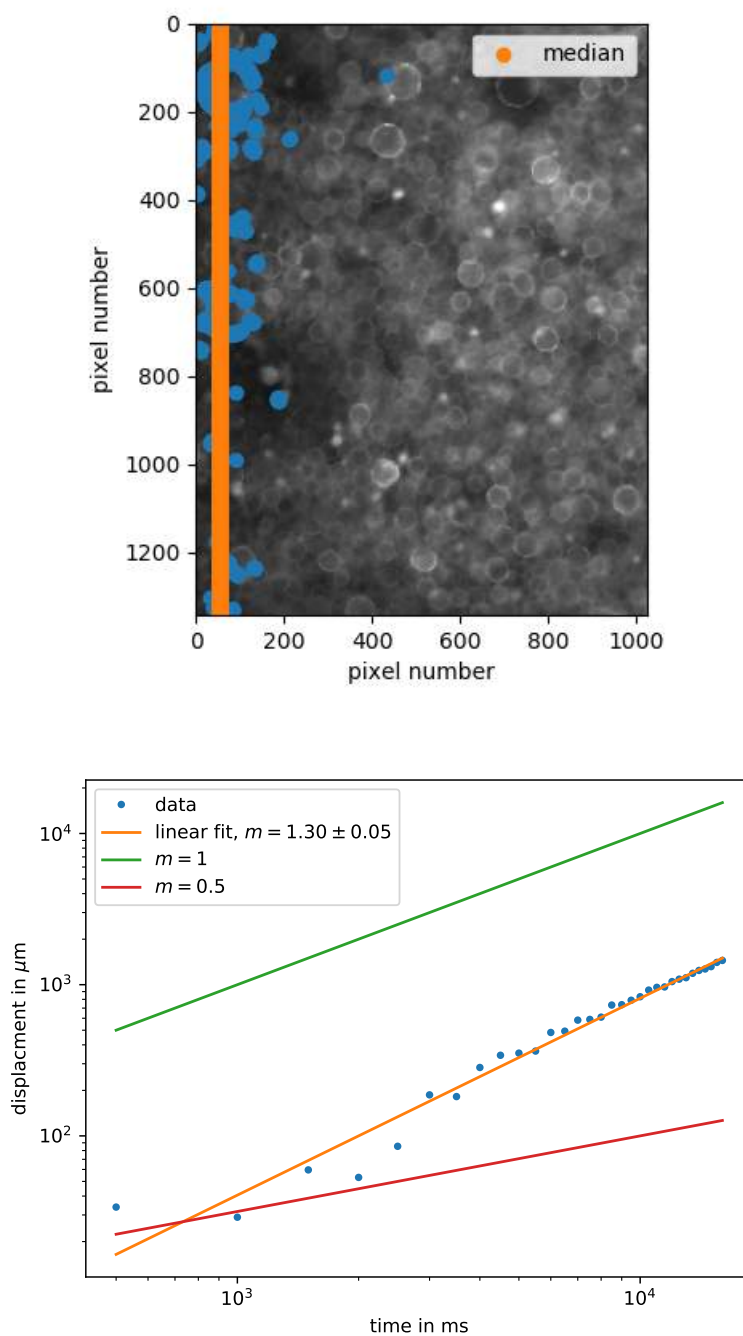


**Figure 3.5:** Top picture shows the calculated median of the blue points. The blue points represent the pixels where the difference is greater than the applied threshold. The bottom picture shows the position of the median over time and the resulting slope of a linear fit. Additionally curves for an ballistic movement (slope  $m = 1$ ) and a diffusive movement (slope  $m = 0.5$ ) are shown for comparison.

## 4 Results

At the beginning the results of the different preparation methods for multilayers are presented. Then the influence of thermodynamic forces is investigated, leading to an emerging wave at phase transition temperature of the respective lipid. It will be shown that the phenomenon is a non-diffusive wave-like propagation of a phase transition in the lipid multilayers.

### 4.1 Formation and characterization of multilayers

In this part the results of the formation of the lipid multilayers by the different methods described in 3.3 will be presented. Each method is investigated with bright-field and fluorescence microscopy revealing the characteristics at the surface. In addition X-ray reflectivity measurements are taken on the substrates by the lab of Prof. Metin Tolan at TU Dortmund.

When conducting experiments with the different methods it became clear that the choice of method had no significant influence on the principle outcome of the experiment. Therefore, the method for displaying the results is chosen based on experimental convenience.

#### 4.1.1 Solvent evaporation

##### Bright-field microscopy

An image of the lipid layers under bright-field microscopy is shown in figure 4.1. The surface is irregularly filled with vesicles. Those vesicles seem to be present in all samples and might be produced by the addition of water to the layers. No distinct structures can be recognized. Nonetheless the non-uniform distribution of vesicles implies defects in the homogeneity.

In some cases an extra electroformation of the system is employed. Figure 4.2 shows two images of a bright-field recording. The first image is before electroformation and the second after the procedure. It can be seen that already small vesicles exist on the lipid layer surface before electroformation but the size and number is highly increased with the treatment.

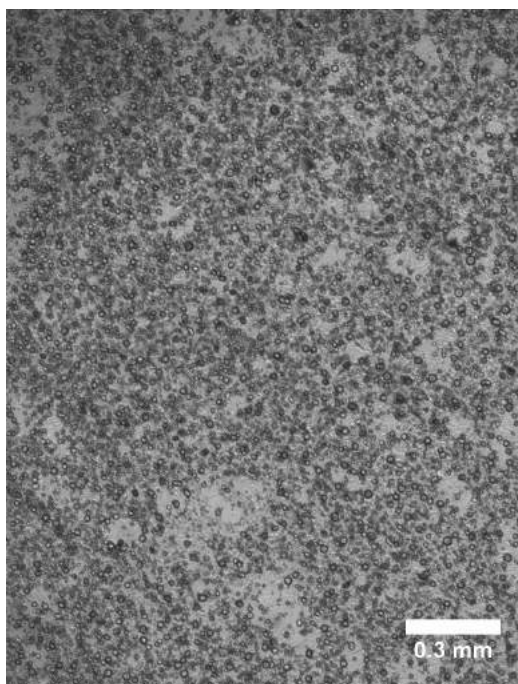


**Figure 4.1:** DMPC lipid layers under bright-field microscopy.

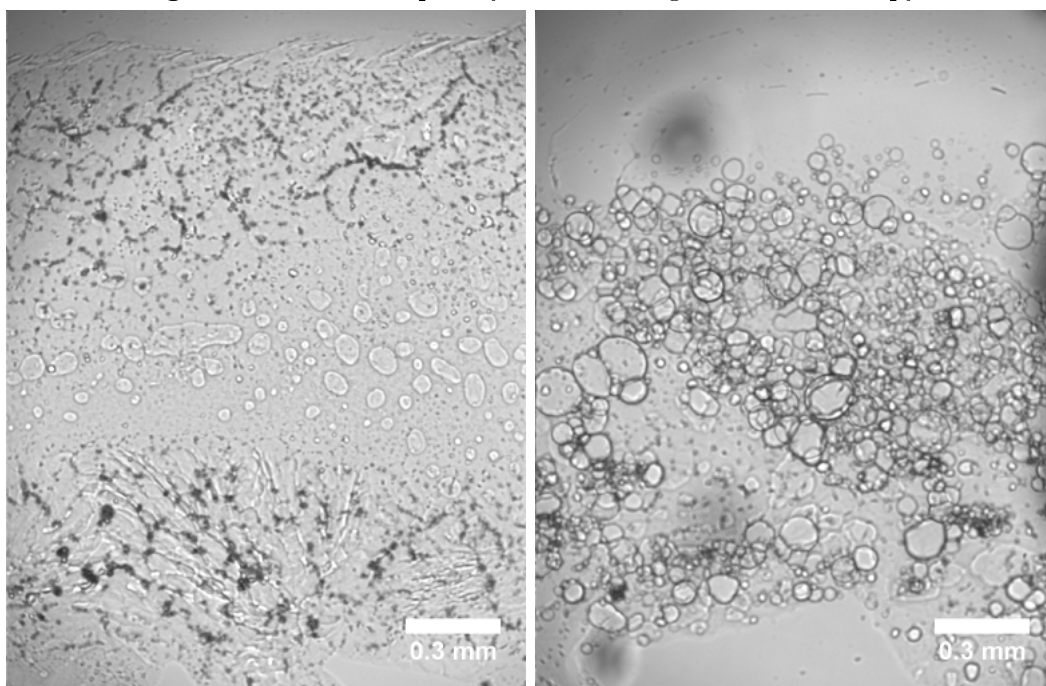


**Figure 4.2:** Bright-field microscopy before (left) and after (right) electroformation. Vesicles are already visible before the process but the number and size are highly increased after the treatment.

### Fluorescence microscopy

For fluorescence microscopy the two different dyes Laurdan and Texas Red are employed. In figure 4.3 an image of lipid layers in fluorescent light is shown. Only the example of Texas Red is given here, since the both dyes show the same structures. The only difference when employing the dyes is the emitted wavelength (color). The colors cannot be distinguished with fluorescence microscopy because the camera only records in gray scales. The dyes are employed for other important properties than their color. They indicate a possible phase transition (see subsection 4.3.2) and also show structures that are not visible by bright-field microscopy (see bright-field investigations in subsection 4.1.2).

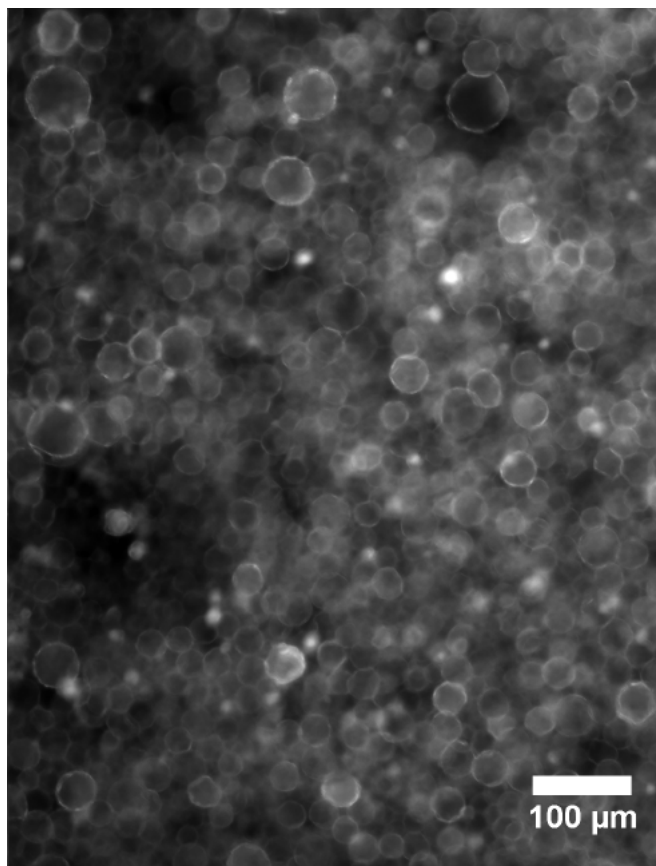


**Figure 4.3:** Fluorescence microscopy of lipid layers with Texas Red after electroformation. The gray scale does not show the color of the dye but it is able to visualize structures that are invisible in bright-field microscopy.

### X-ray reflectivity analysis

In order to characterize the number of lipid layers a X-ray reflectivity analysis has been carried out by the lab of Prof. Metin Tolan. The set-up of the labor diffractometer is described elsewhere [48] and will not be further explained in this thesis. The results give a lipid spacing (head to head) and the total lipid layer count. Three different samples give a spacing of  $d = (54.8 \pm 0.3) \text{ \AA}$  and total lipid layer counts of 22, 23 and 28 lipid bilayers. This clearly states a difference to other authors, where hundreds of lipid layers are expected [45]. A reason for this discrepancy will be given in section 5.1. Nonetheless, no influence on the results are to be expected since the idea is to investigate lipid layers with a layer count greater than one. Hundreds of lipid layers would be helpful but not necessary.

### 4.1.2 Spin-coating

#### Bright-field microscopy

Bright-field microscopy is not employed for spin-coated system because there are too little layers and no visible structures are recognizable.

#### Fluorescence microscopy

Fluorescence microscopy is able to visualize the surface structure of slides with a few layers. A typical picture is shown in figure 4.4. A very homogeneous excitation of light from the surface can be seen, indicating well orientated lipid layers. Single defects that look like scratches and a few bright points are recognizable. Those defects are due to defects in the surface and also a detachment of lipids when flooding the chamber with water resulting in small vesicles.

#### X-ray reflectivity analysis

The same X-ray reflectivity measurements as for the solvent evaporation method are carried out for spin-coated systems. One sample could be investigated with 10mg/ml DMPC spin-coated on an ITO slide. Seven double layers of lipids were measured. This slightly lower number of lipid layers will not have an influence on the here found phenomenon. Nonetheless, higher differences in the layer count could possibly influence the phenomenon. This has not been tested in this thesis.

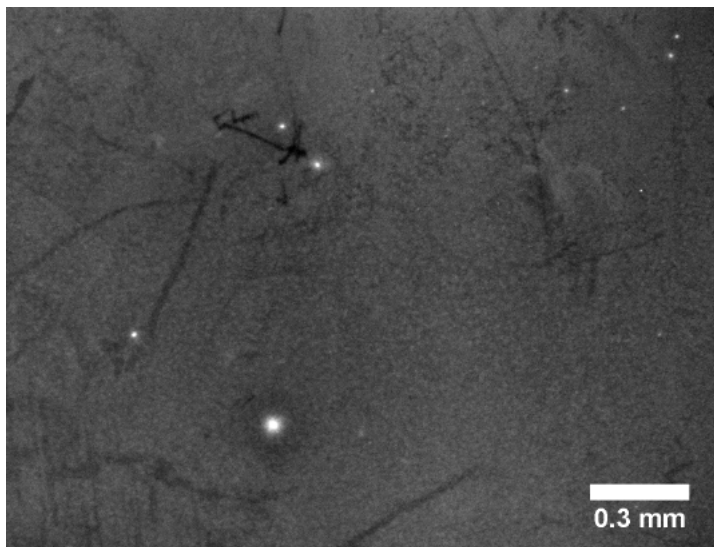


**Figure 4.4:** Fluorescence microscopy of spin-coated lipid layers with Texas Red.

## 4.2 Effects of thermodynamic forces

Thermodynamic forces are employed to excite the lipid layers out of their equilibrium state and investigate how the systems react to those forces. Here two different ways of exciting the system have been carried out. Nonetheless, theory predicts further sources for exciting the lipid layers (mechanical, chemical etc.). The first thermodynamic force is the electric field (discussion in subsection 5.3). Under the influence of an alternating electric field the surface vesicles change their form periodically. In this 2D cross sectional view it appears like an expansion and compression. The second thermodynamic force is temperature and thermal perturbations lead to the extraordinary effect of an emerging wave that will be further investigated.

### 4.2.1 Electric fields

In order to excite the lipid layers with an electric field, alligator clamps are attached to the ITO slides (see 3.4). Alternating voltages of  $U = 2\text{ V} - 4\text{ V}$  with a frequency of  $f = 1\text{ Hz}$  are applied. Since changes in single pictures are difficult to see, a video<sup>1</sup> has been recorded where a periodic change in the form of the surface vesicles according to the applied frequency can be seen.

Electric fields should be able to excite the lipid layers in terms of triggering an acoustic wave in the medium. This could not be observed here. A discussion of reasons and improvements will be held in section 5.3.

<sup>1</sup><https://youtu.be/Krk68gxKeTs>

## 4.2.2 Temperature

To observe the effect of temperature perturbations the samples are heated or cooled. A typical result when heating a spin-coated sample is displayed in figure 4.5. The choice of pictures shows the sample over time while heating. In the top left picture no systematic difference to the picture in figure 4.4 after preparation can be seen. With increasing temperature and time a darkening starting from the bottom can be recognized which is indicated by arrows. This subsequent darkening is observed between  $T = 24.5^\circ\text{C}$  (first picture) and  $T = 26.5^\circ\text{C}$  (last picture). As an additional guide the mean value of all pixels is plotted over time in figure 4.6.

The pixel values represent the brightness of the pictures because the camera only records in gray scales. It can be seen that the intensity decreases over time supporting the findings in the pictures. An excerpt of the full video can be found on youtube<sup>2</sup>.

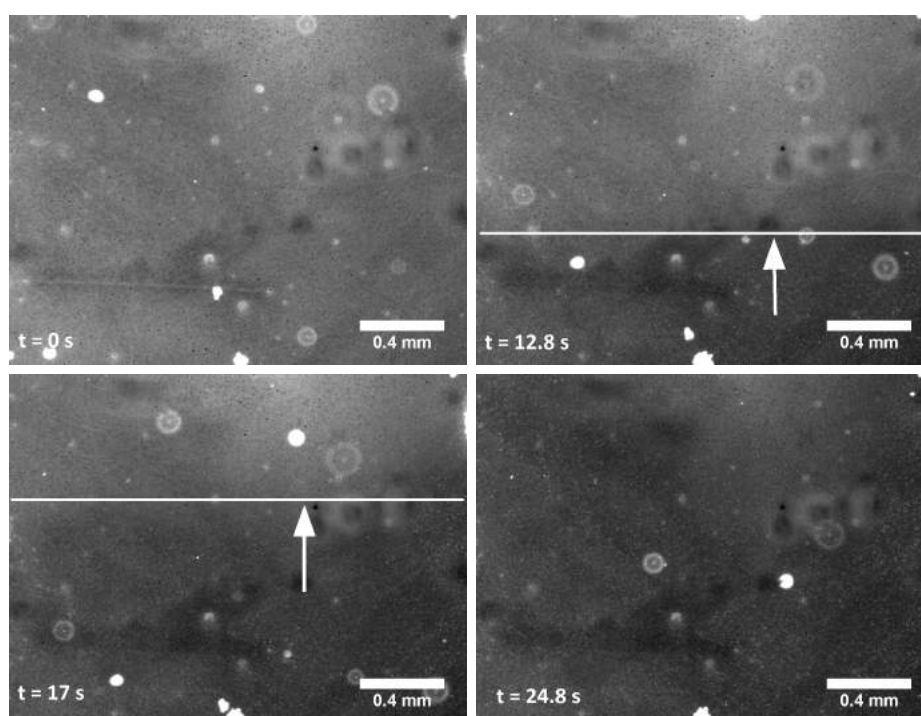


**Figure 4.5:** From the bottom of the pictures emerging wave in spin-coated DMPC layers with Texas Red. Time development from top left ( $t = 0$  s) to bottom right ( $t = 24.8$  s). Arrows indicate wave front.

This subsequent darkening looks like an emerging wave. Such a wave can also be found in systems of solvent evaporation, without the need of fluorescence light (video<sup>3</sup>).

<sup>2</sup><https://youtu.be/bpgHhd4yk4E>

<sup>3</sup><https://youtu.be/0BBIpG3SgWo>

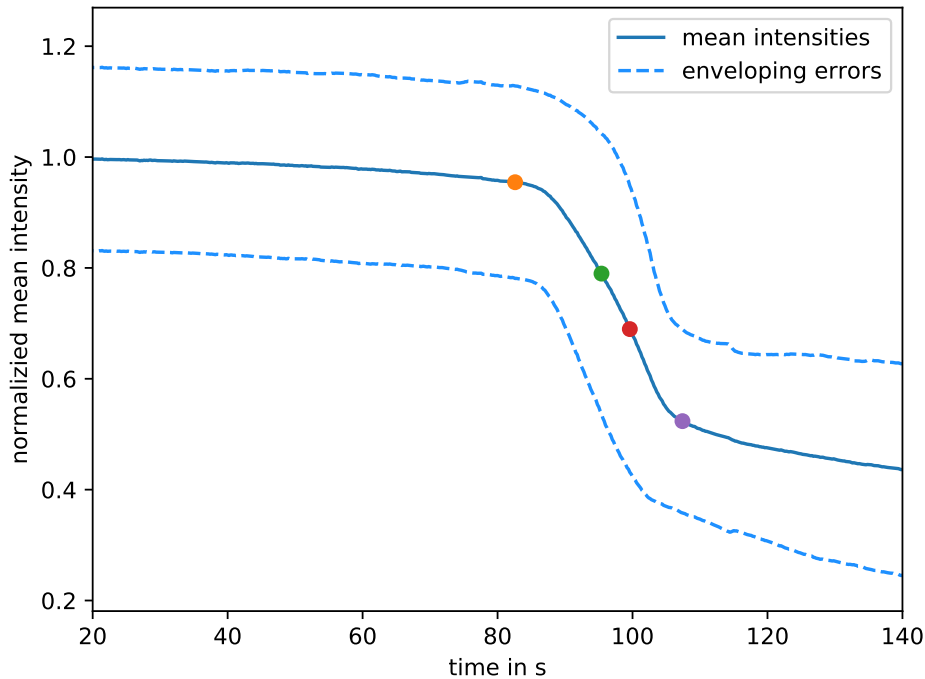


**Figure 4.6:** Mean intensity of each picture. Additional marks for the four pictures shown in figure 4.5. Enveloping error curves show standard deviation of all pixel values. The high deviation is due to a few very bright spots.

In fact, in approximately 50 experiments (not presented) the temperature has been measured when the wave enters the field of view. An emerging of a wave could be found for both situations, cooling and heating the lipid layers.

The temperatures when the wave emerges are around  $(24 \pm 1)^\circ\text{C}$ . Single outliers are also observed. These values hold for DMPC, which has its phase transition temperature at  $24^\circ\text{C}$  [19]. This correlation implies a phase transition of the lipids with the emerging wave.

Additionally, the influence of an electric field during wave propagation is investigated in an experiment (video<sup>4</sup>). DMPC layers are already cooled below  $24^\circ\text{C}$  and the alternating voltage is applied, resulting in no motion of the surface vesicles. Subsequent heating of the lipid layers leads to the known wave phenomenon at phase transition temperature. Instantly as the wave passes, the vesicles start changing their form periodically. This behaviour works vice versa when reversibly cooling the lipid layers from more than  $24^\circ\text{C}$  under the phase transition temperature (not shown).

<sup>4</sup><https://youtu.be/8FPeWfgWo6Q>

It is known that bending rigidity changes significantly when lipids undergo a phase transition [49]. For vesicles this leads to a softening or solidifying of the lipid surface, respectively. Depending on their respective state the vesicles might follow (more fluid phase) the changes in the electric field or do not move (more condensed state). In these experiments an abrupt change of motion can be seen with the emerging wave, strongly indicating a phase transition.

### 4.3 Wave propagation at phase transition

Temperature measurements of the emerging wave and the excitability of the lipid vesicles strongly imply an accompanied phase transition. In the following further experiments are conducted to support this idea.

#### 4.3.1 Thermal threshold of lipid chain length

In order to check if the found wave is a membrane phenomenon, the investigations are extended to the second lipid DPPC. It has a different phase transition temperature ( $T_m = 41\text{ °C}$ ) than DMPC [19]. If the observed phenomenon arose in the water, it would not appear around  $41\text{ °C}$ .

The result of cooling DPPC lipid layers can be seen in this video<sup>5</sup>. Since a wave close to the phase transition temperature is recognizable it can be concluded that the wave is not triggered by water.

A selection of temperatures when the emerging wave was measured in DMPC and DPPC systems is displayed in table 4.1. All results from the table are measured in solvent evaporated samples. Investigations in spin-coated samples give comparable results (see for example figure 4.9). There are several factors that make it difficult to exactly determine the temperature at which the waves emerge. This will become clearer in subsection 4.3.2 and discussed in chapter 5. For now it can be stated that the phenomenon does not arise from water.

---

<sup>5</sup><https://youtu.be/BX3FVb9nLoM>

**Table 4.1:** Selection of temperature values when the wave emerges.

Lipid	Heating/cooling	Temperature T in °C
DMPC	heating	24.0
DMPC	heating	25.0
DMPC	heating	23.0
DMPC	heating	24.0
DMPC	cooling	23.0
DMPC	cooling	25.0
DMPC	cooling	25.5
DMPC	cooling	23.5
DPPC	heating	40.5
DPPC	heating	40.5
DPPC	cooling	41.5
DPPC	cooling	44.0

### 4.3.2 Indication by dyes

Phase transition can be observed by dyes, since their properties react to changes in the lipids layers. Here the results for the two dyes Texas Red and Laurdan are shown.

#### Laurdan

Laurdan is well known to indicate phase transitions by changes in the generalized polarization [50–52]. To investigate the lipid behaviour with the emerging wave, the generalized polarization is measured for different temperatures in a quasi-static experiment (see 3.5). The generalized polarization is calculated from spectra measurements. The results are displayed in figure 4.7.

It can be stated, that between 22.0 °C and 23.5 °C a polarization change ( $\approx -0.25$ ) is recognizable. This indicates a phase transition around these temperatures.

In all other experiments of this thesis the set-up conditions cannot be assumed to be quasi-static. Hence, this measurement is repeated in the regular set-up. The results are shown in figure 4.8. Again a drop in in the generalized polarization can be recognized but the change occurs at a different temperature. Also, the form of the curve differs from figure 4.7.

This differences can be explained with the heating rate and the measurement of the temperature. In figure 4.7 the temperature is set to a specific value followed by 10 min equilibration. In the live measurement of figure 4.8 the set-up is continuously heated. This leads to a different form of the curves. The temperature sensor is placed on top of the chamber. Therefore the sensor reacts faster to heat changes than the lipids in the water inside the chamber do.

## 4 Results

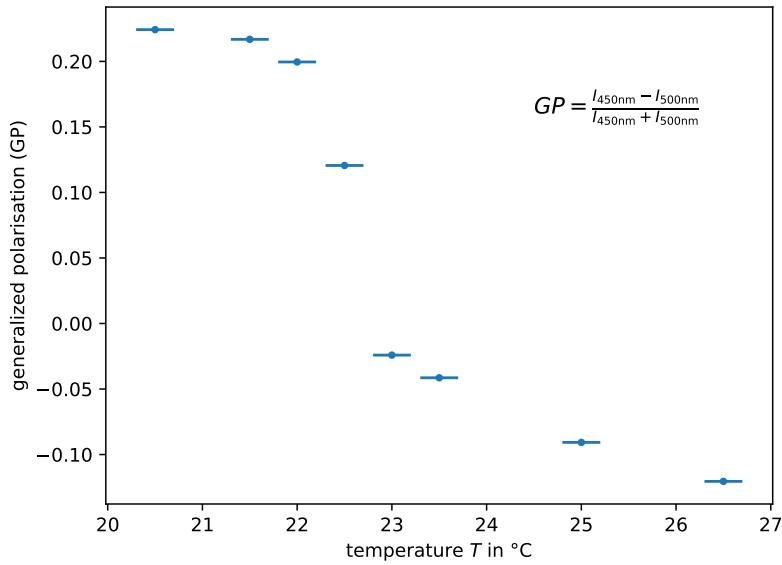


**Figure 4.7:** Generalized polarization (GP) of Laurdan in DMPC layers prepared by solvent evaporation. The generalized polarization is calculated with the intensity values of the wavelengths  $\lambda_B = 450 \text{ nm}$  and  $\lambda_R = 500 \text{ nm}$ . Temperature errors are  $0.2^{\circ}\text{C}$  and GP errors in the order of a few permille.

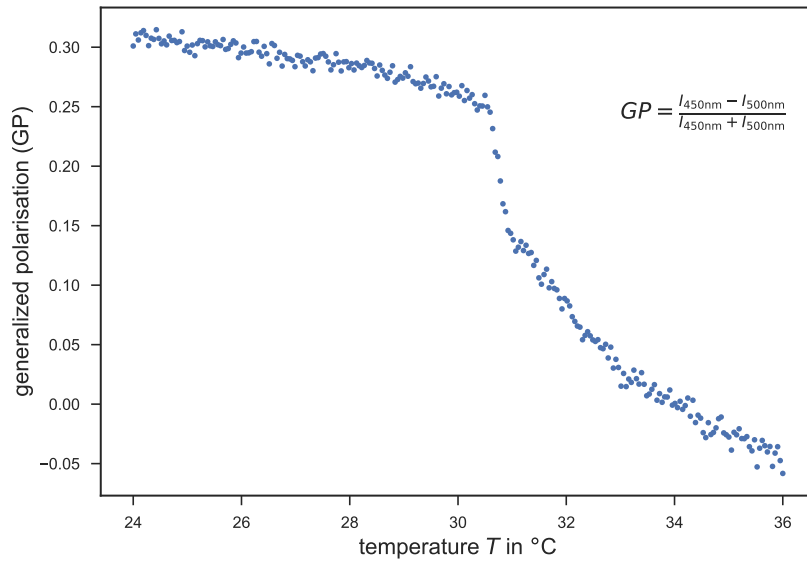


**Figure 4.8:** Generalized polarization (GP) of Laurdan in DMPC layers made by solvent evaporation with rising temperature. The temperature is a linear interpolation between the first temperature  $T = 21^{\circ}\text{C}$  and the last temperature  $T = 36^{\circ}\text{C}$ . The drop of GP is located at a temperature of  $T \approx 30^{\circ}\text{C}$ . Errors are not displayed since error sources are identified with the help of this graph.

## Texas Red

Texas Red is usually not employed to display phase transitions in lipids. Nonetheless, the intensity of Texas Red changes non-linearly with the emerging of a wave (see figure 4.5 for example), which indicates a possible phase transition. In order to quantitatively investigate the behaviour, a spectrum analysis is conducted when the waves emerge. Spectrum analysis is chosen because it reveals more information about the ongoing processes than just e.g. integration of the intensity values. A shift in intensities might not be detected by an integration of intensity values. The results for a spin coated system are shown in figure 4.9. In the top graph the spectra for a set of different temperatures are shown. It can be seen that the intensity decreases significantly between 22 °C and 24 °C. The bottom graph shows the maximal intensity values - which are at 609 nm - for different temperatures. The corresponding values can also be found in table 4.2. From these values a clear drop of intensity of approximately 19 % can be recognized between 23.0 °C and 23.5 °C. Compared to the change in intensity between 20.0 °C and 23.0 °C, which is  $\approx 2\%$ , this confirms the results that have been observed in microscopy.

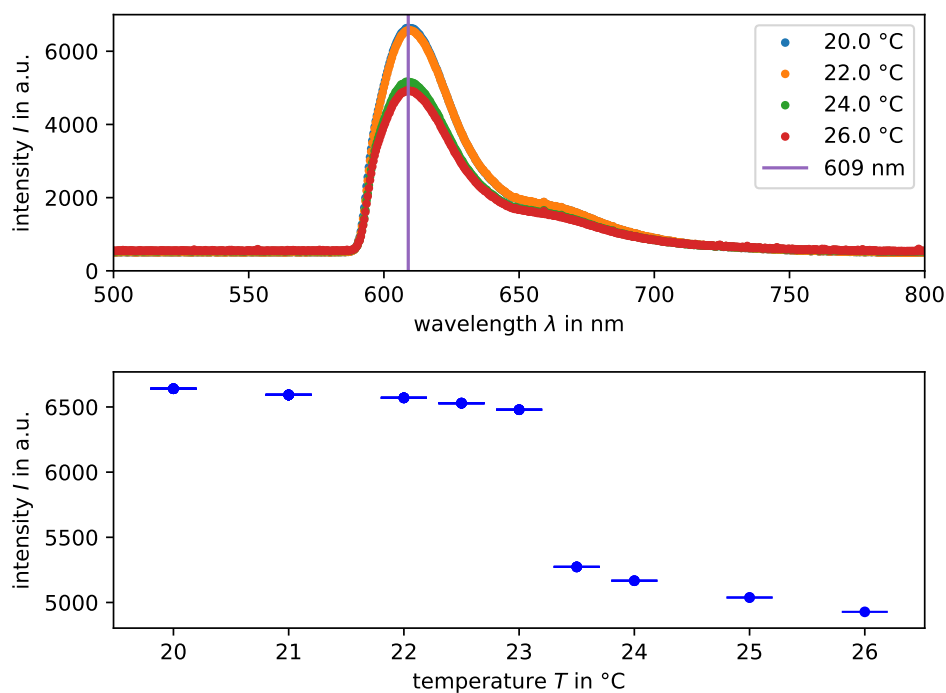


**Figure 4.9:** Measurement of Texas Red spectra in spin coated DMPC layers (top). Intensities at 609 nm for different temperatures indicating phase transition (bottom).

**Table 4.2:** Intensities at 609 nm for different temperatures. Values taken from spectra measurements of spin-coated DMPC slides with Texas Red. Intensity errors are too small to be seen.

Temperature $T$ in °C	Intensity $I$ in a.u.
20.0	6640
21.0	6593
22.0	6570
22.5	6529
23.0	6479
23.5	5273
24.0	5167
25.0	5038
26.0	4928

All these different aspects lead to the conclusion that the observed waves are accompanied and/or triggered by a phase transition. This phase transitions appear reproducible for heating and cooling of the lipid multilayers. The results are invariant with respect to the method of lipid preparation. The choice of lipids do not change the results, too.

## 4.4 Propagation velocity and behaviour

The waves found here are accompanied by a phase transition. In the following the velocity and behaviour of this wave will be examined.

### 4.4.1 Velocity

The mean wave velocity is calculated by hand, meaning that the pictures in which the wave can be seen are counted and divided by the number of pictures times the time span for each picture. This method is employed for many different waves (50-100) in the same and in different samples, for heating and cooling. The majority of velocities are in the range of  $\approx 2$  mm/min to  $\approx 15$  mm/min with a few outliers. A systematic difference between heating and cooling could not be found for DMPC. For DPPC the mean velocities are in the same range as for DMPC but there is an obvious difference in the wave speed when cooling or heating the sample. Examples for each lipid are given in table 4.3.

The influence of the different preparation methods - solvent evaporation and spin coating - for lipid layers is also investigated. The mean velocities of the solvent evaporation method are in the range of approximately 2 mm/min – 15 mm/min where as investigations on seven different waves in spin coated systems show a

range of circa 4 mm/min – 8 mm/min. The similar values for the mean velocities might be explained by the small difference in the number of layers in each sample. X-ray reflectivity analysis reveals that both methods lead to approximately 10 – 30 lipid layers. Since the wave is a propagation of a phase transition in the lipids, it can be assumed that this small difference in the number of layers give a comparable mean velocity of the waves. The fact that a smaller range of mean velocities is measured in the spin-coated system might be due to a smaller number of overall experiments.

**Table 4.3:** Examples of wave velocities for DMPC and DPPC.

Lipid	Heating/cooling	Velocity $v$ in mm/min
DPPC	heating	$4.9 \pm 0.1$
DPPC	cooling	$14.84 \pm 0.05$
DPPC	heating	$9.07 \pm 0.05$
DPPC	cooling	$18.14 \pm 0.05$
DMPC	heating	$10.88 \pm 0.05$
DMPC	cooling	$10.20 \pm 0.05$
DMPC	heating	$9.99 \pm 0.04$
DMPC	cooling	$14.43 \pm 0.04$

### 4.4.2 Non-diffusive behaviour

Analysing the propagation behaviour the waves show a non-diffusive character. The analysis is performed as explained in section 3.6. The wave front is recorded over time and the position of the wave front is plotted in a double logarithmic plot versus time. The slope of the resulting graph is used to discuss the propagation behaviour. Figure 4.10 shows the propagation of the median before processing. Three different parts of the plot are distinguished by two vertical lines. The first and second part show linear slopes which only differ in their respective values. The third part is characterized by a drop in the slope.

At the beginning, when the wave enters the field of view the median is calculated for the front of the wave. Then the median does not follow the wave front because the wave has a physical width. The whole wave has not entered the field of view, yet. Therefore it looks like an acceleration of the wave when the whole wave has entered the field of view. Consequently, this part is not considered in the slope calculation and will be left out in the following. The third part of the picture is caused by the exiting of the wave. After the wave has left, only noise is found in the field of view. This part is also left out and will not be taken into account for the calculation of the slope.

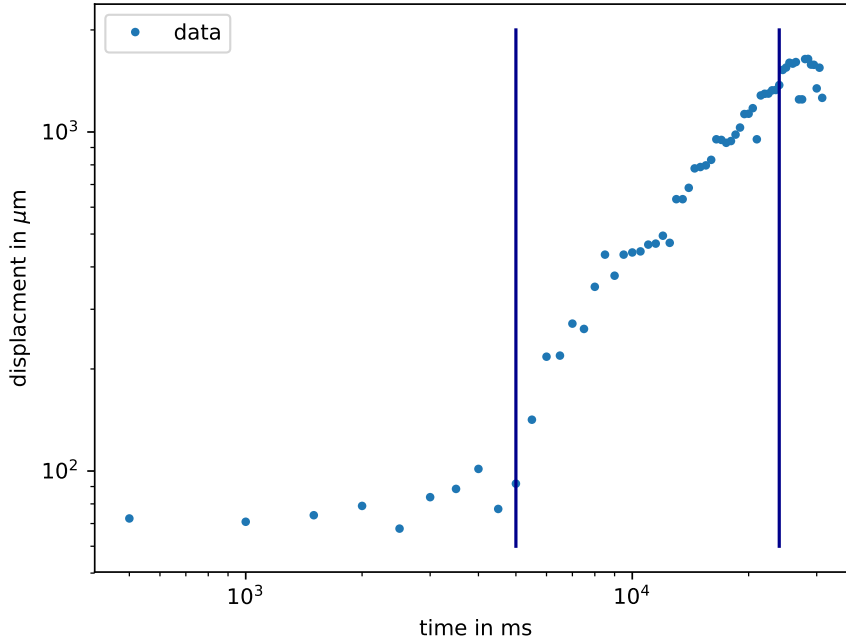


**Figure 4.10:** Non-processed median propagation. Separation of the plot in three parts with two vertical lines. This distinction is made due to artefacts of the entering and exiting of the wave.

Here only a selection of different waves (two out of ten) is presented but it shows the overall behaviour of the investigated waves. The first example in figure 4.11 shows a slope of  $m = 1.30 \pm 0.05$ . The wave was observed while heating the sample. For comparison the slope for a wave that emerged while cooling is shown in figure 4.12. The slope is determined to  $m = 0.98 \pm 0.02$ . In both cases a clear non-diffusive behaviour can be observed (slope  $m > 0.5$ , for explanation see subsection 2.2.3).

An analysis of 10 waves in one sample gave an average slope of  $m_{avg} = 1.3 \pm 0.3$  with a minimal slope of  $m_{min} = 0.79 \pm 0.01$  and a maximal slope of  $m_{max} = 1.8 \pm 0.1$ . Therefore it cannot be clearly stated whether the waves accelerate during propagation or if they move in a ballistic way.

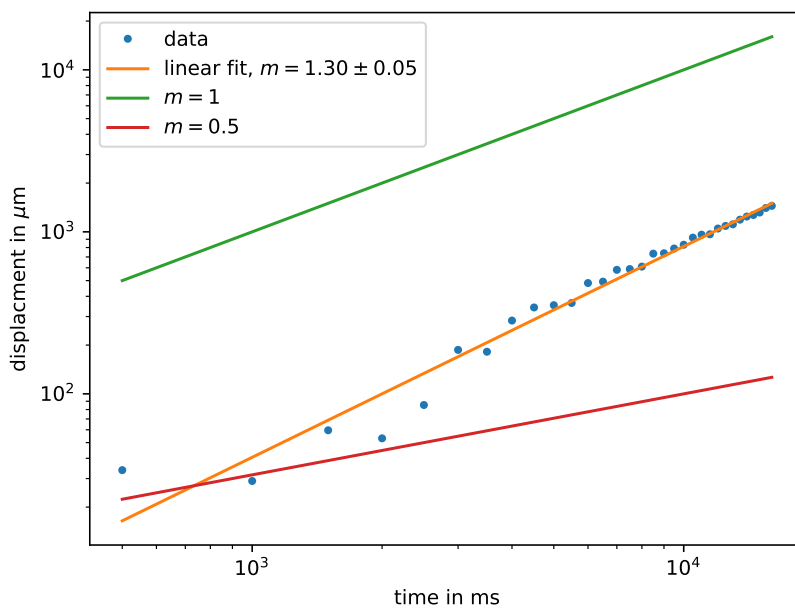


**Figure 4.11:** Time development of median while heating a DMPC sample. The slope of the median values is calculated to  $m = 1.30 \pm 0.05$ .

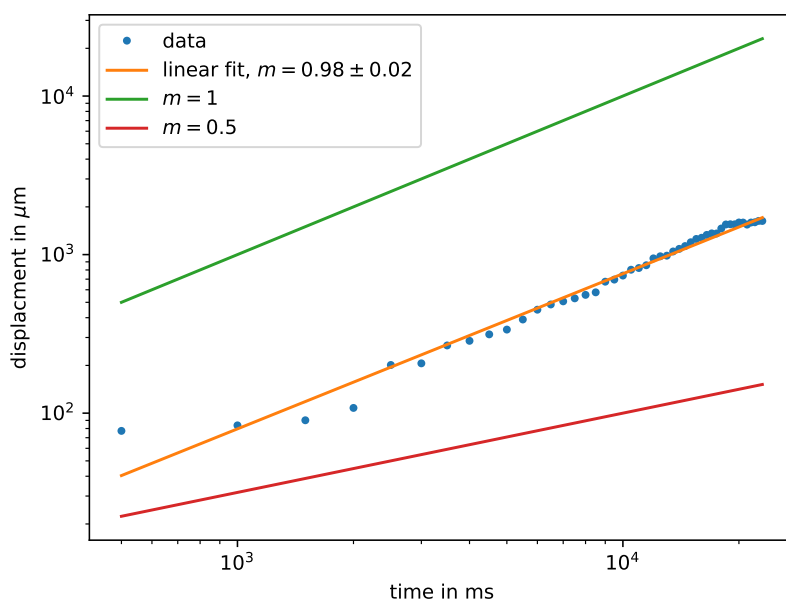


**Figure 4.12:** Time development of median while cooling a DMPC sample. The slope of the median values is calculated to  $m = 0.98 \pm 0.02$ .



## 5 Discussion

### 5.1 Layer counts

When comparing the methods of producing multilayers it has been shown that the methods produce different numbers of lipid layers. The solvent evaporation results in  $\approx 20$  layers – 30 layers, whereas the analysis of one spin-coated sample showed seven layers.

In both cases a different number of lipid layers was expected (a few hundreds for solvent evaporation and 20 for spin-coating). The reasons for this can be found in the conditions when preparing the samples. Solvent evaporation is extremely sensitive to additional streams of any gas because they increase the evaporation and therefore reduce the quality of the layers. Since the preparation of the samples is only possible under fume hoods, additional streams could not be excluded. This led to a significant disturbance of the formation of lipid layers. In consequence only  $\approx 20$  layers – 30 layers were prepared and detected with X-ray analysis.

In the case of spin-coating the formation of lipid layers is sensitive to many different parameters (lipid concentration, speed and time of spinning etc.) [46]. The parameters for this thesis were extracted from experiments with silicon slides of a smaller area (15 mm x 25 mm) than the here used ITO slides (25 mm x 25 mm). Those differences might lead to the lower number (7 instead of 9-17) of lipid layers on the ITO slides.

The accuracy of X-ray analysis is additionally verified by determining the thickness of the ITO layer of the slides. They consist of floating glass on which  $\text{SiO}_2$  is coated with a thickness of 150 Å – 300 Å [53]. Analysis with X-ray diffraction came to a layer thickness of 186 Å – 199 Å measured in two samples, which confirms the statements of the supplier.

### 5.2 Necessary prerequisites

The wave found here has not been observed in other experiments, yet. Therefore it is of special interest which conditions are necessary to cause the wave to emerge.

The main components seem to be the ITO substrate, the lipids, the chemicals and excessive water. Since lipids in layers are the main focus of this work, the lipids will not be substituted by other molecules.

## 5 Discussion

---

Nonetheless, another phenomenon without lipids showing a wave-like phase transition can be found. The freezing of supercooled water is a propagation of a phase transition that will be discussed in section 5.5.2.

### Water

Water is indispensable for the emerging of the wave. Further experiments have been conducted (not presented) where the set-up with lipid layers was prepared but the chamber has not been filled with water. A heating and cooling of the sample did not lead to waves. So water seems to be absolutely necessary. However, it is unclear if a particular level of humidity is already enough to excite waves, too.

To prove that the waves originate from the presence of lipid layers and not from water, two different types of lipids (DMPC and DPPC) were tested. These experiments revealed waves only at the respective phase transition temperature of the lipids. This correlation is satisfactory to state that the waves originate in the presence of lipid layers.

### Solvent

In order to check whether the solvent has an influence on the emerging of the wave, isopropanol was used instead of chloroform. Therefore DMPC powder was dissolved in isopropanol and then spin-coated on the ITO substrate. No differences in the wave behaviour were observable.

In the case of solvent evaporation additionally TFE is added to the lipids and chloroform. The influence of TFE on the emerging of waves is investigated by preparing a sample without adding TFE to the lipid solution. Minor differences in the optical appearance of the resulting lipid layers were observable. After the lipid solution was dried, rings of lipids had formed. Those rings might be caused by the so called coffee-ring effect [54]. Different evaporation rates across the drop lead to a concentration of lipids at the edge of the drop. In samples with TFE no such rings were visible and the overall distribution of lipids looked more homogeneous. Nonetheless, the wave phenomenon appeared reproducible in absence of TFE. From this it can be followed that TFE enhances a homogeneous distribution of lipid layers but is not strictly necessary.

### Substrate

The last parameter to check is the influence of the substrate. Instead of using ITO slides as substrate, slides from regular laboratory glass slides were employed. These slides were treated exactly like the ITO slides. The result was that the wave was found, too. In both cases (ITO and laboratory glass) the surface consists of glass.

In order to check the influence of glass on the emerging wave, silicon slides were employed. DPMC is spin-coated on the silicon slides but no waves were observable. This might be due to the different thermal conductivities of silicon and glass. Silicon has a thermal conductivity of  $149 \text{ W}/(\text{m K})$  [55] and glass has a conductivity of  $0.8 \text{ W}/(\text{m K})$  [56]. The high thermal conductivity of the silicon slides make it impossible to build up a thermal gradient. Without a gradient the waves cannot emerge. The glass slide has a much lower thermal conductivity which results in a thermal gradient over the sample, enabling the wave to emerge. This observation is in accordance with theory. It was stated that a local disturbance is necessary to trigger a wave. A local thermal gradient represents such a disturbance. If the gradient diminishes no excitation of a wave is possible.

## 5.3 Thermodynamic forces

In this part the concept of a thermodynamic force will be briefly revisited. Also, the problems of the temperature measurements are pointed out.

### Electric field

Thermodynamic forces are intensive variables which multiplied by an extensive variable represent an energy or work contribution of the first law. An example for an intensive variable is the voltage  $U$ . The voltage multiplied by the charge  $q$  gives the electric Energy  $E = qU$ . For a plate capacitor the electric field is  $E_e = U/d$ , where  $d$  is the distance between the plates of the capacitor. Therefore the energy can be rewritten as  $E = qE_e/d$ . In this thesis the distance between the ITO slides is kept constant. Consequently, the distance does not influence the thermodynamic force and the electric field can be used as the acting thermodynamic force.

It was not found to be possible to trigger a phase transition wave with an electric field in this thesis. Multiple reasons might play a role in this context. Probably the electric field has to act locally in order to evoke a significant local stimulation. Here, the electrodes covered the whole lipid area so that no local stimulation was possible. An improvement can be achieved by inserting a silver electrode in the chamber and positioning it directly on top of the lipids. Additionally, the form of the alternating electric field possibly has influence on the lipids. Here a sine-wave was employed, which leads to low gradients in the electric field. Perhaps a steeper edge in voltage stimulates the lipids better. For this a sawtooth voltage might be employed. Another problem is the fact that it is unclear where the major drop in voltage actually happens. Since the chamber is filled with water, this might have a major impact on the electric field that is effectively stimulating the lipids.

### Temperature discrepancies

In subsection 4.3.2 the wave is measured in an live-experiment. The drop of GP was recorded for a temperature of  $\sim 30^\circ\text{C}$ . This seems to be a clear contradiction to the statement that the wave emerges at phase transition. In fact this result shows the problems of the temperature measurements in the here used set-up.

Several error sources play a role in this context. The used temperature sensor displays the values with an accuracy of  $0.25^\circ\text{C}$  but in fact the temperature can only be trusted in a range of approximately  $\pm 1^\circ\text{C}$ . This is an estimation for the uncertainty is based on two facts. First the accuracy of the sensor of  $\pm 0.5^\circ\text{C}$ . Second the position of the sensor gives another uncertainty that is estimated with another  $\pm 0.5^\circ\text{C}$ . The sensor is not placed directly at the lipid layers but on top of the chamber. The chamber itself consists of two ITO slides, a spacer, excess water and the lipids. Especially the water is a big heat capacity making measurements on top of the chamber quite inaccurate.

If temperature is measured in a semi-static experiment the values are reliable, but during a live measurement the system is pushed out of equilibrium and temperature gradients are present all over the sample. This cannot be precisely measured with the here used set-up. Therefore the result of  $29.5^\circ\text{C}$  as the temperature when the wave emerges should not be trusted. Nonetheless this result tells many things about the phenomenon and helps interpreting other findings as the varying wave speeds.

## 5.4 Varying wave speeds for DMPC and DPPC

The necessity of temperature gradients for the emerging wave has been pointed out in section 5.2. Many consequences have to be taken into consideration when interpreting the results. For example the different wave speeds for cooling and heating DPPC (see section 4.4). DPPC has its phase transition Temperature at  $T_m^{DPPC} = 41^\circ\text{C}$ . Reaching  $T_m^{DPPC}$  from room temperature  $T_{room} \approx 22^\circ\text{C}$  needs higher gradients than cooling it from above  $T_m^{DPPC}$  to a lower temperature. This is due to heat losses to the surrounding. The effective gradient while heating is much smaller as compared to cooling with the same parameters. This discrepancy can be observed in the wave speeds of DPPC for heating and cooling. Cooling shows a higher velocity as the gradient is higher as well. This behaviour could not be observed for DMPC since DMPC phase transition temperature is  $T_m^{DMPC} = 24^\circ\text{C}$ , which is close to room temperature. No further investigations on the wave speed dependency on temperature gradients have been performed. Therefore it remains unclear why and how the gradients have influence on the wave speed. However, two further predictions can be made, that should be tested in the future. First a higher gradient will lead to a faster wave speed and second a homogeneous heating (no gradient) over phase transition will result in no occurring wave.

## 5.5 Comparable phenomena

The discussion of the results already gave new insights in the understanding of the phenomenon. In the following two examples will be discussed where the here found wave might be a reasonable explanation for the effects.

### 5.5.1 Spreading depression waves

The presented phase transition waves in lipid stacks have striking similarity to the so called spreading depression or spreading depolarization. Spreading depression is a phenomenon that was first found by Leão [2] in the cortex of rabbits. Further investigations came to the conclusion that spreading depression waves propagate in the grey matter of the cortex [1]. It is a wave of active propagation which causes a breakdown of transmembrane ion gradients [1] and depresses spontaneous activity [2]. The typical speed of those waves is around 2 mm/min – 9 mm/min [1].

In this discussion the velocity of both phenomena and the depression of spontaneous electrical activity are compared.

#### Velocity

The velocity of the propagating phase transition was found to be in a range of 2 mm/min – 15 mm/min. In spreading depression the velocity of the waves ranges from 2 mm/min to 9 mm/min. This striking similarity makes it likely that both phenomenon may be triggered by the same causes. Nonetheless, discrepancies can be found when comparing the propagation behaviour.

The speed of the spreading depression is interpreted as a sign of diffusion [57]. So far no studies could be found, that actually tested the diffusive behaviour of the spreading depression. Therefore explaining this phenomenon with a non-diffusive propagation of the phase transition might be possible, too. Although further investigations have to made.

#### Depression of activity

The phenomenon of the depression itself is comparable, too. In spreading depression the passing wave reduces the spontaneous electrical activity of the tissue. Also, it is impossible to excite the tissue with electric fields for several minutes [2].

Here it was found that the emerging wave stops all motion of electrically excitable surface vesicles, when cooling the sample (see subsection 4.2.2). This depression of motion was only reversible with another emerging wave, when heating the sample again. It can be argued that the depression of motion in this thesis is similar to the impossibility to excite tissue in spreading depression.

In this context the behaviour of the spreading depression wave could be explained as follows: the emerging of the spreading depression is a phase transition wave pushing the lipids and the tissue in a phase where no excitation is possible.

Differences can be found in the phenomenon of spontaneous activity and the recovery from depression. The here investigated lipid layers do not show any spontaneous activity. This might be due to the reduced complexity of the model.

A depressed tissue takes several minutes to recover. In this time no further wave is observable. This means that the lipids do not undergo a collective phase transition again but 'slowly' relax to their initial state individually. The reasons remain unclear why only a wave of depression is visible. This questions might be answered by understanding the reasons of the emerging of the depression wave in tissue, which cannot be answered by the approach presented here.

Leão found a gradual depression of activity which is not as sudden as presented in this thesis. Solutions for this discrepancy are speculative but might be found in the high complexity of grey matter tissue. The simple models of this work does not include all parameters of real tissue. The influence of proteins, different lipid mixtures of the membranes can have an major effect on the excitability of a tissue. For example proteins, embedded in the membranes of single cells and layers of lipids are slightly changing the phase diagram of a cell individually and the tissue overall. In conclusion the propagating phase transition of this thesis shows similar characteristics like spreading depression. Those similarities are a adequate starting point to explain spreading depression from a physical point of view. Nonetheless, discrepancy are presented and have to be investigated in future. In order to verify the connection of the phase transition wave and spreading depression, the propagation of the spreading depression wave should be investigated in terms of its diffusive behaviour.

### 5.5.2 Supercooling of water

Supercooling is the effect that matter does not undergo phase transition even though it would be an energetic more desirable state. Examples can be found in normal water that is left over night in the freezer and is not frozen or hand warmers which contain a supersaturated solution. In both cases a mechanical disturbance leads to a phase transition (videos for supercooled water can be watched in [58] and [59]). This induced phase transition appears optically to be very similiar to the here found phase transition wave. A systematic approach on supercooled water can be found in [60].

### Threshold

There the supercooled water is investigated in terms of determining the temperature at which supercooled water freezes spontaneously. The main statement is that supercooling strongly depends on motes in the water. However, influences of mechanical disturbances were also investigated. It was found that mechanical stresses can induce the phase transition. Nevertheless, not all mechanical disturbances lead to the freezing of the super cooled water. This threshold depends on the temperature of the supercooled water. The higher the temperature the stronger the mechanical disturbance had to be. A value for the threshold was not given, since the experiments were only conducted qualitatively. No threshold experiments have been conducted in this thesis, but other authors [12,13] found thresholds for exciting acoustic pulses in lipid monolayers. Hence, these findings seem to be in accordance to the physical approach of thermodynamics.

### Velocity

In general, the development of the ice phase is explained with crystal growth. Aliotta et al. conducted experiments on crystal growth in supercooled water [61]. There the growth of dendrites in the ice phase is measured and taken as the overall propagation of the phase transition. The speed of the growing dendrites was determined to  $\approx 0.5$  cm/s. A decrease in the velocity was also observed, which is a contradiction to the findings of other authors [62–65]. Probably boundary conditions play a role in this set-up.

Even though both phenomena are propagating phase transitions the approach is different. Here, the wave is derived by physical principles, whereas in super cooled water a complex explanation of crystal growth is employed. This is a good starting point for explaining the freezing of supercooled water by physical principles.

Nonetheless different aspects still need further clarification. For example the speed of the phase transition wave in super cooled water is higher ( $\approx 0.5$  cm/s) than in lipids ( $\approx 8$  mm/min). A possible explanation might be given by the lower density of super cooled water compared to lipid membranes [66]. Since linear waves can propagate faster in less dense media (see subsection 2.2.3), the higher speed of the phase transition in supercooled seems plausible.

A propagation of phase transition is found in super cooled water but might be explained less complex with the phenomenon found in this work. The phase transition wave found here can purely be explained by physical principles and does not need complex growing mechanisms. Therefore it seems reasonable to explain the similar observation of freezing of supercooled water with the same principles.



## 6 Conclusion

In this thesis lipid multilayers were investigated under the influence of thermodynamic forces (temperature and electric fields). No significant change in the shape of the lipid layers was observed upon heating or cooling, except close to the melting phase transition temperature. This change is a propagating wave which crossed the microscopic field-of-view.

In the range of detection ( $\approx 1.6$  mm) the propagation of the wave was evident without decay. Image analysis indicated that the propagation ( $x \propto t^\alpha$ , with  $0.8 \leq \alpha \leq 1.8$ ) is not diffusive. The propagation velocity was found to be in the range of 2 mm/min – 15 mm/min in most cases. The thermal gradient appears to have an influence on the propagation velocity. A higher thermal gradient seems to lead to a higher propagation velocity.

Correlation of the wave appearance with the phase transition was shown by the use of two different lipids (DMPC and DPPC). The wave only emerged close to the respective phase transition temperature of the lipids (24 °C for DMPC and 41 °C for DPPC). Further investigations using the two different dyes, Texas Red and Laurdan, confirmed the results of a propagating phase transition. The emission properties (generalized polarization for Laurdan and intensity for Texas Red) changed distinctly upon passage of the wave.

The electric excitability of the lipid layers was investigated, by applying an alternating electric field. A pulsation of the surface vesicles could only be detected, when they were in the fluid phase. However, a propagating wave could not be triggered by the electric field. Explanations are found in the limitations of the experimental set-up rather than for principle reasons.

Since the findings are strongly deduced from thermodynamics, they are compared with known phenomena of propagation waves in spreading depression as well as supercooled water. Although, discrepancies between the phenomena and the propagating wave in lipid multilayers are evident, a propagating phase transition appears to be a promising approach.

To put it in a nutshell the idea of using thermodynamics to investigate biological systems has been successfully extended to lipid multilayers allowing to observe a new phenomenon of an emerging wave that is accompanied by a phase transition. In the spirit of explaining life based on physical laws the observations are compared to spreading depression and supercooled water, where a reasonable agreement can be found.



## Bibliography

- [1] J.P. et al. Dreier. Recording, analysis, and interpretation of spreading depolarizations in neurointensive care: Review and recommendations of the cosbid research group. *Journal of Cerebral Blood Flow and Metabolism*, 37:1595–1625, 2016.
- [2] Aristides A. P. Leão. Spreading depression of activity in the cerebral cortex. *Journal of Neurophysiology*, 7(6):359–390, 1944.
- [3] K. Pearson. *The Grammar of Science*. Number Bd. 20 in Contemporary science series. Walter Scott, 1892.
- [4] A. L. Hodgkin and A. F. Huxley. A quantitative description of membrane current and its application to conduction and excitation in nerve. *J Physiol*, 117(4):500–544, Aug 1952.
- [5] B. C. Abbott, A. V. Hill, and J. V. Howarth. The positive and negative heat production associated with a nerve impulse. *Proceedings of the Royal Society B: Biological Sciences*, 148(931):149–187, Feb 1958.
- [6] I. Tasaki, A. Watanabe, R. Sandlin, and L. Carnay. Changes in fluorescence, turbidity, and birefringence associated with nerve excitation. *Proc Natl Acad Sci U S A*, 61(3):883–888, Nov 1968.
- [7] K Iwasa, I Tasaki, and R. Gibbons. Swelling of nerve fibers associated with action potentials. *Science*, 210(4467):338–339, oct 1980.
- [8] Albert Einstein. *Einstein the formative years, 1879–1909 (Einstein Studies)*. Birkhäuser, 2014.
- [9] W. Hanke, K. Kaufmann, and A. Corcia. *Ion channel fluctuations in pure lipid bilayer membranes: Control by voltage*. Caruaru, Brazil, 1989.
- [10] K. Kaufmann. *Action Potentials and Electrochemical Coupling in the Macroscopic Chiral Phospholipid Membrane*. Caruaru, Brazil, 1989.
- [11] K. Kaufmann. *On the role of the phospholipid membrane in free energy coupling*. Caruaru, Brazil, 1989.
- [12] Shamit Shrivastava and Matthias F. Schneider. Opto-mechanical coupling in interfaces under static and propagative conditions and its biological implications. *PLoS ONE*, 8(7):e67524, Jul 2013.

## Bibliography

---

- [13] Bernhard Fichtl and Matthias F. Schneider. Biological signaling by interfacial sound pulses. a physics approach, 2016.
- [14] Carina Fedosejevs. Acoustic pulses in lipid mono- and multilayers. Master's thesis, Technical University Dortmund, 2017.
- [15] A. Einstein. Theorie der Opaleszenz von homogenen Flüssigkeiten und Flüssigkeitsgemischen in der Nähe des kritischen Zustandes [adp 33, 1275 (1910)]. *Annalen der Physik*, 14(S1):368–391, 2005.
- [16] L.D. Landau and E. M. Lifshitz. *Statistical Physics: Volume 5*. Pergamon Press Ltd., 1980.
- [17] Alberts B., Johnson A., Lewis J., et al. *Molecular Biology of the Cell, Fourth Edition*. Garland Science, New York, 2002. Available from: <https://www.ncbi.nlm.nih.gov/books/NBK26871>; accessed 20-Sept-2017.
- [18] Pschyrembel, editor. *Klinisches Wörterbuch (German Edition)*. Walter de Gruyter & Co, 260 edition, 2004.
- [19] Inc. Avanti Polar Lipids. Chemical structure of DMPC and DPPC. DMPC: <https://avantilipids.com/product/850345/>, DPPC: <https://avantilipids.com/product/850355/>. Online; accessed 20-Sept-2017.
- [20] Dimitrios Bitounis, Raphaelle Fanciullino, Athanassios Iliadis, and Joseph Ciccolini. Optimizing druggability through liposomal formulations: New approaches to an old concept. *ISRN Pharmaceutics*, 2012:1–11, 2012.
- [21] Gerald H. Pollack and Wei-Chun Chin, editors. *Phase transitions in cell biology*. Springer, 2008.
- [22] Anthony A. Hyman and Kai Simons. Beyond oil and water – phase transitions in cells. *Science*, 337(6098):1047–1049, 2012.
- [23] W. Schrader, H. Ebel, P. Grabitz, E. Hanke, T. Heimburg, M. Hoeckel, M. Kahle, F. Wenthe, and U. Kaatz. Compressibility of lipid mixtures studied by calorimetry and ultrasonic velocity measurements. *The Journal of Physical Chemistry B*, 106(25):6581–6586, 2002.
- [24] D. Steppich, J. Griesbauer, T. Frommelt, W. Appelt, A. Wixforth, and M. F. Schneider. Thermomechanic-electrical coupling in phospholipid monolayers near the critical point. *Phys. Rev. E*, 81:061123, Jun 2010.
- [25] S. Shrivastava and M. F. Schneider. Evidence for 2D Solitary Sound Waves in a Lipid Controlled Interface and its Biological Implications. *ArXiv e-prints*, May 2014.
- [26] S. Shrivastava, K. H. Kang, and M. F. Schneider. Solitary shock waves and adiabatic phase transition in lipid interfaces and nerves. 91(1):012715, January 2015.

- 
- [27] B. Fichtl, S. Shrivastava, and M. F. Schneider. Protons at the speed of sound: Predicting specific biological signaling from physics. *Scientific Reports*, 6:22874, May 2016.
- [28] Horst Stöcker, editor. *Taschenbuch der Physik : Formeln, Tabellen, Übersichten*. Deutsch, Frankfurt am Main, 5., korrigierte Aufl., Nachdr. edition, 2007.
- [29] R. Lüllmann-Rauch. *Taschenlehrbuch Histologie*, volume 3. Georg Thieme Verlag, 2009.
- [30] Anthony Mescher. *Junqueira's Basic Histology: Text and Atlas, Thirteenth Edition*. McGraw-Hill Education / Medical, 2013.
- [31] Renate Lüllmann-Rauch, editor. *Histologie*. Georg Thieme Verlag, 2012.
- [32] T. Scarabino and U. Salvolini. *Atlas of Morphology and Functional Anatomy of the Brain*. Springer Berlin Heidelberg, 2006.
- [33] Alice S. Pakurar and John W. Bigbee. *Digital Histology: An Interactive CD Atlas with Review Text*. Wiley-Liss, 2004.
- [34] OpenStax. Anatomy & physiology, Nov 2017. <https://cnx.org/contents/FPtK1z mh@8.108:kwbeYj9S@4/Bone-Structure>.
- [35] Joseph R. Lakowicz. *Principles of fluorescence spectroscopy*. Springer, New York, 2006.
- [36] ThermoFisher Scientific. Product page of texas red, Nov 2017. <http://www.thermofisher.com/order/catalog/product/T1395MP>.
- [37] G. G. Stokes. On the change of refrangibility of light. *Philosophical Transactions of the Royal Society of London*, 142(0):463–562, Jan 1852.
- [38] L.A. Chen, R.E. Dale, S. Roth, and L. Brand. Nanosecond time-dependent fluorescence depolarization of diphenylhexatriene in dimyristoyllecithin vesicles and the determination of "microviscosity". *The Journal of Biological Chemistry*, 252(7):2163–2169, April 1977.
- [39] F. Jähnig. Structural order of lipids and proteins in membranes: evaluation of fluorescence anisotropy data. *Proc Natl Acad Sci U S A*, 76(12):6361–6365, Dec 1979.
- [40] T. Parasassi, F. Conti, M. Glaser, and E. Gratton. Detection of phospholipid phase separation. a multifrequency phase fluorimetry study of 1,6-diphenyl-1,3,5-hexatriene fluorescence. *The Journal of Biological Chemistry*, 259(22):14011–14017, Nov 1984.
- [41] T. Parasassi, G. De Stasio, A. d'Ubaldo, and E. Gratton. Phase fluctuation in phospholipid membranes revealed by laurdan fluorescence. *Biophysical Journal*, 57(6):1179–1186, 2017/08/16 1990.

## Bibliography

---

- [42] T. Parasassi and E. Gratton. Membrane lipid domains and dynamics as detected by laurdan fluorescence. *Journal of Fluorescence*, 5(1):59–69, 2017/08/17 1995.
- [43] Leanna M. Levine, Marshall L. Michener, Mihaly V. Toth, and Barry C. Holwerda. Measurement of specific protease activity utilizing fluorescence polarization. *Analytical Biochemistry*, 247(1):83 – 88, 1997.
- [44] M. Seul and M.J. Sammon. Preparation of surfactant multilayer films on solid substrates by deposition from organic solution. *Thin Solid Films*, 185(2):287 – 305, 1990.
- [45] Ziad Khattari, Sebastian Köhler, Yihui Xu, Sebastian Aeffner, and Tim Salditt. Stalk formation as a function of lipid composition studied by x-ray reflectivity. *Biochimica et Biophysica Acta (BBA) - Biomembranes*, 1848(1, Part A):41 – 50, 2015.
- [46] Ulrike Mennicke and Tim Salditt. Preparation of solid-supported lipid bilayers by spin-coating. *Langmuir*, 18(21):8172–8177, 2002.
- [47] Miglena I. Angelova and Dimiter S. Dimitrov. Liposome electroformation. *Faraday Discuss. Chem. Soc.*, 81:303–311, 1986.
- [48] Benedikt Nowak. *Lipidmembranen unter Druck - Untersuchungen an der Festkörper-Flüssigkeits-Grenzfläche*. dissertation, TU Dortmund, 2014.
- [49] Beate-Annette Brüning, Sylvain Prévost, Ralf Stehle, Roland Steitz, Peter Falus, Bela Farago, and Thomas Hellweg. Bilayer undulation dynamics in unilamellar phospholipid vesicles: Effect of temperature, cholesterol and trehalose. *Biochimica et Biophysica Acta (BBA) - Biomembranes*, 1838(10):2412 – 2419, 2014.
- [50] S. A. Sanchez, M. A. Tricerri, G. Gunther, and E. Gratton. Laurdan generalized polarization: from cuvette to microscope. In A. Méndez-Vilas and J. Díaz, editors, *Modern Research and Educational Topics in Microscopy*, pages 1007 – 1014. FORMATEX, 2007.
- [51] L. A. Bagatolli and E. Gratton. Two-photon fluorescence microscopy observation of shape changes at the phase transition in phospholipid giant unilamellar vesicles. *Biophys J*, 77(4):2090–2101, Oct 1999.
- [52] Faith M Harris, Katrina B Best, and John D Bell. Use of laurdan fluorescence intensity and polarization to distinguish between changes in membrane fluidity and phospholipid order. *Biochimica et Biophysica Acta (BBA) - Biomembranes*, 1565(1):123 – 128, 2002.
- [53] Sigma-Aldrich. Product page of ito slides, Nov 2017. [http://www.sigmaaldrich.com/catalog/product/aldrich/703176?lang=de&region=DE&cm\\_sp=Insite-\\_-recent\\_fixed-\\_-recent5-2](http://www.sigmaaldrich.com/catalog/product/aldrich/703176?lang=de&region=DE&cm_sp=Insite-_-recent_fixed-_-recent5-2).

- 
- [54] Robert D. Deegan, Olga Bakajin, Todd F. Dupont, Greb Huber, Sidney R. Nagel, and Thomas A. Witten. Capillary flow as the cause of ring stains from dried liquid drops. *Nature*, 389:827 EP –, Oct 1997.
- [55] C. Y. Ho, R. W. Powell, and P. E. Liley. Thermal conductivity of the elements. *Journal of Physical and Chemical Reference Data*, 1(2):279–421, 1972.
- [56] Saint-Gobain. Glass properties, Dec 2017. <http://www.saint-gobain-sekurit.com/glossary/glass-properties>.
- [57] M.A. Dahlem and S.C. Müller. Reaction-diffusion waves in neuronal tissue and the window of cortical excitability. *Annalen der Physik*, 13(7-8):442–449, 2004.
- [58] ESRFsynchrotron. Watch supercooled water freeze, Dec 2017. [https://youtu.be/DpiUZI\\_3o8s](https://youtu.be/DpiUZI_3o8s).
- [59] mrsciguy. Supercooled water, Dec 2017. [https://youtu.be/DpiUZI\\_3o8s](https://youtu.be/DpiUZI_3o8s).
- [60] N. Ernest Dorsey. The freezing of supercooled water. *Transactions of the American Philosophical Society*, 38(3):247–328, 1948.
- [61] Francesco Aliotta, Paolo V. Giaquinta, Rosina C. Ponterio, Santi Prestipino, Franz Saija, Gabriele Salvato, and Cirino Vasi. Supercooled water escaping from metastability. *Scientific Reports*, 4:7230 EP –, Nov 2014. Article.
- [62] M.E. Glicksman and A.O. Lupulescu. Dendritic crystal growth in pure materials. *Journal of Crystal Growth*, 264(4):541 – 549, 2004. Proceedings of the Symposium - Progress in Crystal Growth.
- [63] Chris Unger and W. Klein. Nucleation theory near the classical spinodal. *Phys. Rev. B*, 29:2698–2708, Mar 1984.
- [64] Izumi Yoshizaki, Takehiko Ishikawa, Satoshi Adachi, Etsuro Yokoyama, and Yoshinori Furukawa. Precise measurements of dendrite growth of ice crystals in microgravity. *Microgravity Science and Technology*, 24(4):245–253, May 2012.
- [65] A.A. Shibkov, M.A. Zheltov, A.A. Korolev, A.A. Kazakov, and A.A. Leonov. Crossover from diffusion-limited to kinetics-limited growth of ice crystals. *Journal of Crystal Growth*, 285(1):215 – 227, 2005.
- [66] D. E. Hare and C. M. Sorensen. The density of supercooled water. ii. bulk samples cooled to the homogeneous nucleation limit. *The Journal of Chemical Physics*, 87(8):4840–4845, 1987.



# Eidesstattliche Versicherung

Ich versichere hiermit an Eides statt, dass ich die vorliegende Bachelorarbeit mit dem Titel "Waves in lipid layers" selbständig und ohne unzulässige fremde Hilfe erbracht habe. Ich habe keine anderen als die angegebenen Quellen und Hilfsmittel benutzt sowie wörtliche und sinngemäße Zitate kenntlich gemacht. Die Arbeit hat in gleicher oder ähnlicher Form noch keiner Prüfungsbehörde vorgelegen.

Ort, Datum

Unterschrift

## Belehrung

Wer vorsätzlich gegen eine die Täuschung über Prüfungsleistungen betreffende Regelung einer Hochschulprüfungsordnung verstößt handelt ordnungswidrig. Die Ordnungswidrigkeit kann mit einer Geldbuße von bis zu 50 000 € geahndet werden. Zuständige Verwaltungsbehörde für die Verfolgung und Ahndung von Ordnungswidrigkeiten ist der Kanzler/die Kanzlerin der Technischen Universität Dortmund. Im Falle eines mehrfachen oder sonstigen schwerwiegenden Täuschungsversuches kann der Prüfling zudem exmatrikuliert werden (§ 63 Abs. 5 Hochschulgesetz - HG -).

Die Abgabe einer falschen Versicherung an Eides statt wird mit Freiheitsstrafe bis zu 3 Jahren oder mit Geldstrafe bestraft.

Die Technische Universität Dortmund wird ggf. elektronische Vergleichswerkzeuge (wie z.B. die Software "turnitin") zur Überprüfung von Ordnungswidrigkeiten in Prüfungsverfahren nutzen.

Die oben stehende Belehrung habe ich zur Kenntnis genommen.

Ort, Datum

Unterschrift